

The Host Galaxies of Narrow-Line Seyfert 1s: Nuclear Dust Morphology and Starburst Rings

R. P. Deo¹, D. M. Crenshaw¹ & S. B. Kraemer²

ABSTRACT

We present a study of the nuclear morphology of a sample of narrow- and broad-line Seyfert 1 galaxies (NLS1's and BLS1's) based on broad-band images in the *Hubble Space Telescope* archives. In our previous study, we found that large-scale stellar bars at > 1 kpc from the nucleus are more common in NLS1's than BLS1's. In this paper we find that NLS1's preferentially have grand-design dust spirals within ~ 1 kpc of their centers. We also find that NLS1's have a higher fraction of nuclear star-forming rings than BLS1's. We find that many of the morphological differences are due to the presence or absence of a large-scale stellar bar within the spiral host galaxy. In general, barred Seyfert 1s tend to have grand-design dust spirals at their centers, confirming the results of other researchers. The high fraction of grand-design nuclear dust spirals and stellar nuclear rings observed in NLS1's host galaxies suggests a means for efficient fueling of their nuclei to support their high Eddington ratios.

Subject headings: galaxies:active - galaxies:nuclei - galaxies:Seyfert - galaxies:morphology

1. Introduction

Seyfert galaxies (Seyfert 1943) are the most luminous type of active galaxy found in the nearby ($z \lesssim 0.1$) universe. They have typical bolometric luminosities $\sim 10^{43} - 10^{45}$ erg s⁻¹, with $M_B > -21.5 + 5 \log h_0$ (Schmidt & Green 1983) as the accepted criterion for distinguishing a Seyfert nucleus from a quasar. Their spectra are dominated by high-ionization atomic

¹Department of Physics and Astronomy, Georgia State University, Atlanta, GA 30303; deo@chara.gsu.edu and crenshaw@chara.gsu.edu

²Catholic University of America, and the Exploration of the Universe Division, NASA's Goddard Space Flight Center, Code 667, Greenbelt, MD 20771; stiskraemer@yancey.gsfc.nasa.gov.

emission lines. Khachikian & Weedman (1974) showed that there are two distinct classes of Seyfert galaxy: type 1 Seyferts with broad (FWHM $> 1000 \text{ km s}^{-1}$) permitted emission lines and superposed narrow (FWHM $\lesssim 500 \text{ km s}^{-1}$) emission lines from forbidden and permitted transitions; while in type 2 Seyferts broad permitted emission lines are absent. Osterbrock (1977, 1981) introduced further classifications from 1.2 to 1.9 with numerically larger types having weaker broad-line components relative to the narrow lines. Using spectropolarimetry, Miller & Antonucci (1983) noticed that in NGC 1068 the broad-line region can be seen in polarized light, leading to the idea that the nature of the central continuum source is similar in both types of Seyferts.

Osterbrock & Pogge (1985) coined the term *Narrow-Line Seyfert 1s* (NLS1's) to denote Seyferts 1s with spectra generally like those of classical Seyfert 1s (strong Fe II, [O III] $\lambda 5007$, $\lambda 4959$ relatively weak compared to hydrogen Balmer series) but with permitted line widths much narrower than typical Seyfert 1s. Goodrich (1989) specified that all NLS1's have $\text{FWHM}(\text{H}\beta) < 2000 \text{ km s}^{-1}$, and this is now the currently accepted criterion to distinguish NLS1's from BLS1's. The emission characteristics of NLS1's place them on one extreme of eigenvector 1 of Boroson & Green (1992), which was determined from principal component analysis (PCA) of a large sample of low-redshift AGN. The PCA analysis confirmed that strong Fe II, weak [O III] and narrow H β lines are the defining characteristics of the NLS1 class in the optical regime.

The current widely accepted model for AGN consists of a supermassive black hole (SMBH) accreting matter via an accretion disk. For NLS1's, the current paradigm is that NLS1's possess black holes of relatively modest mass ($\leq 10^7 M_{\odot}$) that are being fed at or close to the relative Eddington accretion rate (Pounds, Done & Osborne 1995). This view is supported by recent observational results that indicate that NLS1's possess significantly smaller black hole masses than their broad-line counterparts (Mathur, Kuraszkiwicz, & Czerny 2001; Wandel 2002; Peterson *et al.* 2004). In this scenario, the narrow-line widths are simply due to the smaller black hole mass.

In order to fuel AGN, matter must be transported all the way from kiloparsec scales to the central engine. Thus the matter must lose almost all of its angular momentum via some process. One possibility involves mergers or tidal interactions with neighboring galaxies (Toomre & Toomre 1972; Adams 1977). However studies of environments of Seyfert galaxies show no evidence for a statistical excess in number of companion galaxies or any recent merger events (De Robertis, Yee, & Hayhoe 1998) in Seyfert galaxies as compared to normal galaxies. Another process that has received considerable attention is gas inflow along a galactic stellar bar (Simkin, Su, & Schwarz 1980). However most observational studies have found similar fraction of bars in Seyferts and normal galaxies (Heckman 1980; Simkin, Su,

& Schwarz 1980; Ho, Filippenko & Sargent 1997; Mulchaey *et al.* 1997; Mulchaey & Regan 1997). Since there is strong evidence that most normal galaxies contain inactive SMBH (Kormendy & Richstone 1995), this indicates that while gas may be transported to the inner kiloparsec via large-scale stellar bars, there are other factors that contribute to the presence of nuclear activity.

Shlosman *et al.* (1990) proposed the bar-within-bar fueling scenario, where the secondary gas/dust bar develops due to non-axisymmetric instabilities in the gas disk within the inner kiloparsec. Maiolino *et al.* (2000) found evidence for gas motion along a secondary bar-like structure within ~ 100 pc of the central engine in the Seyfert 2 Circinus galaxy. However it appears that either gaseous/dusty secondary bars are fairly rare among Seyfert galaxies or they are relatively small (≤ 100 pc) and we are not yet able to see them due to limited resolution at the distances of most nearby Seyferts (tens of Mpc). Secondary stellar bars are apparently not that uncommon in nearby galaxies (see, Erwin & Sparke 2002, 2003).

Perhaps the most efficient way to detect gaseous inflow to the nucleus is through the extinction caused by its embedded dust. *HST* optical and IR images indicate that only 10-20% of Seyfert galaxies show nuclear dust bars (Regan & Mulchaey 1999; Martini & Pogge 1999; Pogge & Martini 2002). Instead, the *HST* images reveal that most ($\sim 80\%$) Seyfert galaxies show nuclear dust spirals (Regan & Mulchaey 1999; Pogge & Martini 2002; Martini *et al.* 2003a). However Martini *et al.* (2003b) find that nuclear dust spirals in Seyfert galaxies are not statistically more numerous than those in normal galaxies. Thus, it is unclear exactly how the dust spirals fuel the AGN and what mechanism(s) control the onset of nuclear activity. Although these structures are common to both barred and unbarred Seyfert galaxies, all of the “grand-design” nuclear dust spirals (*i.e.*, those with two long symmetric arms) are found in barred galaxies only (Martini *et al.* 2003b). These grand-design nuclear spirals appear to connect to dust lanes on the leading edge of the large-scale stellar bars.

If the high accretion rate paradigm for NLS1’s is correct, it suggests that the fueling of the AGN is more efficient in NLS1’s than in their BLS1 counterparts. In Crenshaw, Kraemer & Gabel (2003) (hereafter, CKG03), we provided evidence that NLS1 nuclei are hosted mostly in barred Seyfert galaxies as compared to BLS1 nuclei: 65% of the NLS1’s have bars, while only 25% of BLS1’s have bars. These large-scale stellar bars typically begin at ~ 1 kpc from the nucleus and extend to 5 – 10 kpc. They represent an efficient means of transporting large amounts of gas and dust to the inner kiloparsec region, which can presumably support large accretion rates. However we did not study the inner regions (< 1 kpc) of the BLS1’s and NLS1’s, where establishing a connection between Seyfert 1 type and inner morphology would be even more crucial for understanding the fueling of the active

nucleus.

The motivations for this paper came from the need to understand the nuclear structures that exist within the central regions of NLS1’s. There are no previous studies comparing NLS1 and BLS1 samples for differences in nuclear morphology. Many of the earlier studies (Martini & Pogge 1999; Regan & Mulchaey 1999) were focused mainly on Seyfert 1.8 to Seyfert 2 galaxies. Pogge & Martini (2002) and Martini *et al.* (2003a) included about equal numbers of Seyfert 1’s and 2’s and investigate the differences between Seyfert 1’s and 2’s. We note that in surveys of nuclear regions of both active and normal galaxies with *HST* (Martini & Pogge 1999; Regan & Mulchaey 1999; Pogge & Martini 2002; Martini *et al.* 2003b) and ground-based imaging studies (Erwin & Sparke 2002), it was found that nuclear dust spirals are seen in similar frequencies in *both* active as well as inactive galaxies. Hence it is not clear if nuclear spirals are indeed efficient in fueling the central source. Further, Martini *et al.* (2003a) find that barred galaxies (either active or inactive) preferentially show a grand-design type of nuclear morphology, while unbarred ones show tightly-wound nuclear spirals. Since host galaxies of NLS1’s are found to be barred from CKG03, we might expect to see grand-design as the preferred nuclear morphology for NLS1’s.

2. Sample Selection and Analysis

2.1. Sample Selection

Our sample contains the *HST* broadband (primarily F606W) Wide Field Planetary Camera 2 (WFPC2) images of Seyfert 1 galaxies obtained in the snapshot survey of Malkan *et al.* (1998). This is a uniform sample of 91 Seyfert 1 galaxies with $z \leq 0.039$ derived mainly from the compilation of Véron-Cetty & Véron (2001). A typical exposure for each snapshot was 500s, and nearly all of the galaxies fell on the PC chip, which has a resolution element of $\sim 0.''1$. The number of useful NLS1’s in this sample is small (13/91); we excluded MARK 335, as it appears as a point source in the WFPC2 image, leaving 12 NLS1’s out of 91 Seyfert 1’s. We did not use the five additional NLS1’s at higher redshifts from our previous study (see Table 1 in CKG03) as we do not have enough resolution at their distances to study nuclear characteristics. We have also not used UGC 05025 which is a NLS1 with z of 0.026 as the F814W exposure time is just 80 secs and the nuclear region is not well exposed. However we note that this galaxy is barred. Not all galaxies in the sample had their centers within the PC chip; following is a list of these: F1146 (WF2), PKS 0518-458 (WF4), WAS 45 (WF4), UM 614 (WF2). These are all BLS1’s and hence have little effect on our results. We decided to not include IR 1319-164 in our analysis as most of the galaxy is outside the PC chip in the WFPC2 field of view on the sawtooth side.

We compiled the redshift (z), axis ratio (b/a), the Hubble stage (T) and the absolute blue magnitude, M_B^0 from NED for the whole sample. M_B^0 is computed from the corrected asymptotic blue magnitude B_T^0 (corrected for interstellar extinction and the K-correction). We used $B_T^0 - M_B^0 = 5 \log cz/H_0 + 25$, with $H_0 = 71 \text{ km s}^{-1} \text{ Mpc}^{-1}$, (Spergel *et al.* 2003). There are galaxies for which we had to assign a value to the numerical Hubble stage index (T), this value was assigned by looking at the morphological classification given as part of the basic data for an object in NED and the table describing the coding of morphological types in the Third Reference Catalogue of Bright Galaxies (de Vaucouleurs, G. *et al.* 1991, hereafter RC3). We have also used The de Vaucouleurs Atlas of Galaxies by Buta, Corwin and Odewahn (in preparation) to assign these values. The values of B_T^0 were selected only from RC3 for consistency. The axial ratio (b/a) were chosen from the RC3 data section provided in NED.

Table 1 shows our sample and its properties. The first column gives the name of the galaxy, the second column gives the redshift of the galaxy from CKG03, and the third column gives the RC3 axial ratio (b/a). The fourth column gives the numerical Hubble stage index (T). The fifth column gives the corrected absolute blue magnitude (M_B^0) computed as given above. The sixth column gives the Seyfert 1 class, *i.e.*, whether the galaxy is a NLS1 or a BLS1. The seventh column gives the large-scale morphology as classified in this paper. The eighth column gives the nuclear morphology classification for each galaxy. Three galaxies had main morphology classifications that could not be defined. These are HEAO 2106-098 (point source), MARK 40 (?), MARK 335 (point source). IR 1319-164 was not included in the analysis as most of the galaxy is outside the PC field of view. This resulted in a sample of 87 Seyfert 1's where both large-scale and nuclear structures could be classified.

We tested the sample for selection biases that may have been introduced due to the heterogeneous nature of our sample. Figure 1 shows the histogram plots of the four host galaxy parameters. The histogram with solid boundary line shows the BLS1 sample (75/87 objects), while the shaded histogram with dashed boundary line shows the NLS1 sample (12/87 objects). In Table 2 we list the representative numbers that describe the sample. The spread (σ) reported are standard deviations for the sample in question.

The sample as a whole (87 Seyfert 1's) have a median Hubble stage index of 1.0, moderately high inclinations of 46.37° and median redshift of 0.024. When we break up the sample into NLS1 and BLS1 classes based on their H_β FWHM (done in CKG03), we see that the NLS1's are slightly more face-on and have a median T of 3.0 as compared to BLS1's which are more edge-on and have a median T of 1.0. The NLS1's are also 0.73 mag. less luminous than BLS1's in the median, which is close to the standard deviation of both groups. All of the differences are smaller than the quoted spreads of the sample. However, we discuss their

possible impact towards the end of §3.

2.2. Analysis

We retrieved all the images from the *HST* archives, which were calibrated with the standard HST pipeline. Since this is a snapshot survey, we only had single frames per galaxy and hence we employed a routine written in IDL to detect and remove cosmic rays. This routine is written specifically for handling WFPC2 data and is tuned for the PC chip. The routine scans the input image for pixels affected by cosmic rays and iteratively discards them, replacing them with average values of pixels in a box centered on the pixel being discarded. The routine also estimates the sky background simultaneously by selecting various peripheral sections of the input image. This option can be turned off in case the galaxy covers the whole of PC, which is the case for most images. Various parameters of the routine control the selection of scanning box size and how to distinguish a faint star from a cosmic ray hit. We also replaced bright foreground stars within the image with a square area on the opposite side of the image, with the line joining the two sections passing through the center of the galaxy. We made sure that none of these areas contained any dust structures. It should be noted that none of these foreground stars were close to the centers of the galaxies being studied. This process was required so that the image enhancement process used would not be affected by the presence of areas of large intensity apart from the central point source. Since we are looking for dust structures near the nuclear source, the cleaner the image, the better the contrast enhancement. Residual cosmic rays were examined and cleaned by eye using a combination of IRAF and IDL tools.

We have employed the method used by Pogge & Martini (2002) to enhance the contrast of dusty structures. This process has been called “structure mapping” and is based on the Richardson-Lucy (R-L) deconvolution process. The structure map is the correction image that emerges from the second iteration of an R-L image reconstruction. It highlights unresolved and marginally resolved structures, as the first-order smooth structures are removed. One starts with a good estimate of the *HST* point spread function (for WFPC2 detectors) and uses it to perform an operation similar to unsharp masking via division. One divides the original image with a PSF-convolved version of the original image, multiplying the resulting image with the transpose of the PSF. This results in an image which contains the high frequency components enhanced in contrast. The resultant image forms the second-iteration corrector image in a R-L deconvolution process (see Pogge & Martini 2002). It is crucial that a properly matched PSF be used to generate these structure maps.

We used 2-D Gaussian fits to the saturated cores of the Seyfert 1s to determine the

location of the central source on the chip, and then generated PSFs by using the TinyTim software (Krist & Hook 1999). The form of the *HST* WFPC2 PSF depends on the following parameters in the order of importance: filter used for the observations, the location on WF or PC detector, the secondary mirror focus position, and the color of object being observed. The latter two parameters were not of great importance, as the final structure map did not show significant improvement in quality when these parameters were tweaked. Most of the galaxy centers were not near any of the available observed PSFs for WFPC2, hence using TinyTim was the only way to get reasonable PSFs. PSF subtraction was attempted but yielded inconclusive results. Information is essentially lost in the saturated core. To attempt subtraction, the PSFs were scaled to the intensity of the central source and embedded in image sections the same size as the original image being worked on. Many images had saturated cores and we estimated best fit 2-D profiles by looking at 1-D cross-sections through the core and fitting the wings to estimate the scale factor. The fits were also judged based on the quality of output structure maps. Since structure maps are quite sensitive to large variations in brightness levels in pixels, performing PSF subtraction and then forming a structure map from the resulting image was not practical.

Final processed structure maps are shown in Figure 2 (see Malkan *et al.* (1998) for the original images). The figures are arranged in the same order as the galaxy name in Table 1. For each galaxy, we show the structure map of a 600 x 600 pixel region of the PC chip which avoids the overscan regions. The first and third rows show these full structure map sections, while rows two and four show the nuclear regions of these structure maps zoomed to appropriate size to facilitate display of nuclear structure. The zoomed nuclear regions for each galaxy are below the full structure map image. In the figure, each image shows the size of the region in arcseconds on the vertical axis, as well as the corresponding projected size of the image in kiloparsec (assuming $H_0 = 71 \text{ km s}^{-1} \text{ Mpc}^{-1}$, see Spergel *et al.* 2003) in the top title. The structure map images are bounded by lower and upper thresholds to display faint structures properly. The images are also color inverted. Dusty, high extinction areas appear white, while emission regions appear dark. Compass markers indicate the North and East directions on the image. The color bar at bottom is provided as a guide to how the brightness and contrast of the image was stretched between the applied upper and lower thresholds.

The first two authors independently classified the nuclear structures without prior knowledge of the Seyfert type (*i.e.*, BLS1 or NLS1) or the main galaxy morphology. We looked at the original image as well as the structure map in the process. We chose the following notation for our classification: DS for nuclear dust spiral, DB for nuclear dust bar, A for amorphous dust clouds, DL for large-scale dust lane passing in front of the central source and ND for no significant dust structure. We also noticed that several galaxies showed star-

forming rings inside the central kiloparsec and in two cases (MARK 334 and MARK 1044) star-forming nuclear spiral arms. We called the starburst nuclear spirals, SBS and the nuclear rings, NR. Further, we classified the dust spirals (DS) into two secondary classes: GD for two arm grand-design spirals and FL for flocculent multi-armed spirals. The nuclear dust spirals which could not be classified into these two classes were bunched together with the notation “?” for their secondary classification. We call a nuclear dust spiral grand-design (GD), if it has two distinct symmetric dust spiral arms. Examples in Figure 2 include MARK 1126, MARK 42 and MARK 766. TOL 2327-027 is a spectacular example of this class. The flocculent dust spirals (FL) were defined to be those that showed more than two distinct spiral arms peppered with puffy gas and dust clouds. This class essentially bunches together the classes TW and LW from Martini *et al.* (2003a). Examples of this class include: ESO 323-G77, ESO 354-G4, MARK 1330, MARK 590 and MARK 609. NGC 2639 is a good example of the multi-arm nature of these spirals. There were other cases with only a single dust arm visible (*e.g.*, MCG8-11-11, NGC 6104, MARK 744), the galaxy has a high inclination which prevented a clean classification (*e.g.*, F51), or showed slightly chaotic grand-design like structure with a hint of a dust bar-like structure (*e.g.*, IC 1816, MARK 334, UM146). These were not given any special secondary classification and were grouped together in a category called “?”. Our class A corresponds to class C (for chaotic) from Martini *et al.* (2003a). In the final classification, we cross-checked and reassigned appropriate classes to the few cases where we originally disagreed. The Appendix at the end of the text of this paper lists all the galaxies and the reasons for their individual classifications.

Also during the classification process we noticed that a few of the galaxies had been previously classified as a spiral (class S) in CKG03, when on inspection of structure-mapped images and WFPC2 mosaics, they looked to be barred spirals (class SB). For example, in the PC2 image of ESO 215-G44 in Malkan *et al.* (1998), the large-scale bar is not obvious, but can be seen clearly in a structure map. Other such cases have been recorded in the Appendix. These galaxies have since been reclassified as SB in Table 1. In CKG03, they had concluded that excluding point sources, ellipticals, irregular and unclassified (main morphology class) galaxies (12 out of 97): 34% (29/85) of spiral Seyfert 1’s are barred, 65% (11/17) of NLS1’s are barred, and 26% (18/68) of BLS1’s are barred, indicating a high fraction of barred host galaxies for NLS1’s. With our revised classification, we now conclude from the CKG03 sample of 97 Seyfert 1’s that, excluding point sources, ellipticals, irregular and unclassified (main morphology class) galaxies (12 out of 97), we now have: 47% (40/85) of spiral Seyfert 1’s are barred, 76% (13/17) of NLS1 host galaxies are barred and 40% (27/68) of BLS1 host galaxies are barred. Thus the incidence of large-scale bars in NLS1’s is still much larger than that in BLS1’s.

3. Results

In Table 1, we give the results of our classifications. Column 7 gives the large-scale morphology based on the structure maps and WFPC2 mosaic images (see CKG03 for the original classifications). Column 8 gives the nuclear morphology classification for each galaxy. Within the parenthesis in column 8 is the secondary nuclear classification. Galaxies that were not given a formal secondary dust spiral classification are included in the category “?”.

Table 3 and Table 4 shows the frequencies of these classes as fractions; number counts for galaxies are given in parenthesis along with one sigma uncertainties assuming a binomial distribution (since all the classes are independent and each structure is either present in the galaxy or not). The distributions are given for the entire sample of 87 Seyfert 1’s, as a function of class (NLS1 *vs.* BLS1) and as a function of the host galaxy morphology (barred spirals *vs.* unbarred spirals). Table 4 shows the distributions for GD, FL and the undefined (“?”) categories of dust spirals. All of the entries in this table come from the galaxies that show dust spirals (Table 3, column 3) as their primary nuclear morphology.

Figure 3 shows the bar plots for each class of nuclear structure. For each graph, the vertical axis is frequency of the structure and the horizontal axis has the various classes as in Table 3. On the top of each bar is the fraction corresponding to the class being presented. The plots on the right side correspond to comparison of barred vs unbarred galaxies in the sample while the plots on the left side correspond to NLS1’s *vs.* BLS1’s.

We do not see nuclear dust bars, in agreement with Pogge & Martini (2002). Erwin & Sparke (2002, 2003) demonstrate how stellar secondary bars can be uniquely identified with help of isophotal analysis and unsharp-masking. Since structure mapping is similar to unsharp-masking, we could have noticed the presence of secondary stellar bars, but we did not detect any.

Table 3 and Figure 3 show that 83% of NLS1’s and 67% of BLS1’s have nuclear dust spirals, implying that nuclear spirals are the favored morphological features, in agreement with Martini *et al.* (2003b). In Table 4, we see that 80% (8/10) of NLS1’s with nuclear dust spirals have grand-design type nuclear spirals as compared to 32% (16/50) for BLS1’s with nuclear dust spirals. We also see that, 69% (22/32) of barred spirals with nuclear dust spirals have grand-design structure, compared to 7% (2/28) in the unbarred spirals. Since the sample of Seyferts with barred galaxy morphology is more than doubled by adding barred BLS1 (27/75) to the NLS1 (9/12) sample, and yet the percentage of grand-design nuclear dust spirals (22/32, 69% of barred Seyfert 1 sample with dust spirals) remains almost the same as for NLS1’s (8/12, 67%), we conclude that large-scale stellar bars are the principal driver of the grand-design dust structure. Even though we have only 12 NLS1’s in our

sample, 9 are barred and we see that 8 of them show grand-design nuclear dust spirals. This lends support to the idea that higher fueling rates in NLS1’s are helped by the transfer of gas on kiloparsec scale via large-scale stellar bars which almost always form grand-design dust spirals within 1 kpc of the nuclei of NLS1’s.

During the classification process for nuclear dust structures, we noticed that several galaxies in our sample showed nuclear star formation in the form of stellar nuclear rings or star-forming nuclear spiral arms. ESO 323-G77, IR 1249-131, MARK 42, MARK 493, MARK 530, MARK 744, MARK 896, MARK 1044, NGC 1019, NGC 6212, NGC 7469, TOL 2327-027 and WAS 45 show nuclear star-burst rings (see Figure 2). MARK 334 and MARK 1044 show nuclear spiral arms with star forming sites embedded in them. Table 3 and bar plots in Figure 3 show that 42% (5/12) of NLS1’s show recent star-formation in nuclear rings. One out of these (MARK 1044) has star formation in the nuclear spiral instead of the nuclear ring. In comparison only 12% (9/75) BLS1’s show recent nuclear star formation in the form of nuclear rings. Again only one (MARK 334) shows star formation in the nuclear spiral arms. We do not think that we have missed any inner stellar rings due to the presence of luminous point sources, unless they are very small. The size of the saturated point source is typically much less than 0."5 and at a median z of 0.024; 0."5 (about 10 pixels) corresponds to about 245 pc at resolution of *HST*. We note that all galaxies that host stellar nuclear rings also show grand-design dust spirals and are barred galaxies; see the NR category in the top right plot in Figure 3.

As mentioned previously, the NLS1’s and BLS1’s in our sample show slight differences in their luminosities (0.73 mag.) , inclinations (11.1°) and Hubble stage (2 stages). It is unlikely that these differences have an impact on our ability to detect the nuclear dust morphology and the presence of nuclear rings.

As we have discussed, both observational and theoretical studies show that the presence or absence of a large-scale stellar bar is the principal driver in determining the nuclear morphology. Since it is difficult to detect large-scale bars in highly inclined system, we tested the robustness of our results by excluding galaxies with inclinations greater than 60° . With this constrain, we have 10 NLS1’s and 66 BLS1’s. From this reduced sample, 9 out of 10 NLS1’s (90%) have nuclear dust spirals. Out of these 9 dust spiral, 7 are grand-design (77%) and one flocculent (11%). In comparison, out of 66 BLS1’s, 48 (73%) show nuclear dust spirals. 15 (23%) of these are grand-designs, while 22 (33%) are flocculents. Further, 8/10 (80%) NLS1’s are barred compared to 27/66 (41%) BLS1’s, showing that NLS1’s are more barred than BLS1’s as for the whole sample. Of the total 35 barred galaxies in this reduced sample of 76 galaxies, 21 (60%) have grand-design nuclear spirals, while 4 (11%) are flocculents. Of the 32 unbarred galaxies in this reduced sample, 19 (59%) show flocculent

nuclear spiral, while one shows grand-design (3%). Further, 5/10 (50%) NLS1’s show nuclear rings, while only 9/66 (14%) of BLS1’s show nuclear rings. Thus the difference in inclination does not seem to contribute to a selection bias for bars.

We noted above that intrinsically NLS1 and BLS1 samples differ in their absolute blue magnitudes. We suppress the contribution of the nuclear point source when creating the structure maps. Any residual contribution to the magnitude due to the Hubble type of the galaxy or the nature of its bulge, will be very much smaller than the initial luminosity difference present in the original image between the point source and the rest of the galaxy. Thus we think our ability to detect faint dusty structures near point sources has not been affected by the intrinsic magnitude differences between the NLS1 and BLS1 host galaxies.

Thus in conclusion the trends we see in our original sample of 87 galaxies seem to be robust against small variations in the host galaxy parameters.

4. Discussion

Our statistical analysis shows that the grand-design nuclear dust spirals are largely present in barred galaxies, which is consistent with previous studies. We have also found that NLS1 galaxies, which are thought to have relatively high accretion rates, tend to show large scale stellar bars, nuclear rings and grand-design nuclear spirals. Are grand-design nuclear spirals indeed more efficient in fueling the central nucleus?

Here we summarize from the literature the theoretical efforts to answer this question. The linear density wave theory (Goldreich & Tremaine 1978, 1979) forms the theoretical underpinnings of hydrodynamical simulations of gas inflow in barred galaxies. Englmaier & Shlosman (2000) showed that the morphology of the nuclear gas/dust spiral depends on two factors: central mass concentration and sound speed in the gas (*i.e.*, gravitational potential and amount of turbulence present in the gas disk). The pitch angle (angle between the spiral arm and a tangent to a circle intersecting with the spiral arm at radius R) of the spiral is thus dependent on these two factors and ideally one can probe these factors based on the morphological features of the nuclear disk. We note that this has not been done so far by any study. In the presence of a large-scale stellar bar potential, the hydrodynamical simulations from several studies (Englmaier & Shlosman 2000; Patsis & Athanassoula 2000; Jogee *et al.* 2002; Maciejewski *et al.* 2002; Maciejewski 2004a,b) show that inflow along leading-edges of the stellar bars form “grand-design” type spiral structure in the central kiloparsec. It seems from the discussions in these papers that the presence of the large-scale stellar bar potential overwhelms the effects of nuclear gravitational potential and turbulence throughout most of

the central kiloparsec. This effect is reflected in the tendency of tightly-wound nuclear spirals to avoid barred galaxies in agreement with our observations (see FL category in bottom right bar plot in Figure 3). The merging of grand-design nuclear spiral arms with the leading-edge bar shocks indicates that the nuclear spiral is not decoupled from the large-scale stellar bar, and that the nuclear spiral pattern is *maintained* by the bar potential.

Maciejewski *et al.* (2002) show that the velocity field of the gas in grand-design nuclear spirals has a large negative divergence. This is indicative of strong shocks along the curving dust lanes, which are needed to drive gas down to the scale of tens of parsec. The merging of grand-design spiral arms with leading-edges of large-scale bars occurs regardless of underlying nuclear potential or sound speed in gas, hinting at the importance of large-scale bars in driving the grand-design nuclear spiral. Simulations of Maciejewski (2004b) indicate that the average inflow rates at ~ 1 kpc are $\sim 0.7 M_{\odot} \text{ yr}^{-1}$, at 250 pc they decrease to $\sim 0.2 M_{\odot} \text{ yr}^{-1}$, and at a distance of 40 pc they are $\sim 0.03 M_{\odot} \text{ yr}^{-1}$ in models with both a central SMBH of $10^8 M_{\odot}$ and a large-scale stellar bar. The inflow at distances of 40 pc is ~ 20 times smaller in models without a black hole. In the absence of a secondary bar on scales of hundreds of parsec, one probably needs a strong main bar potential to drive spiral shocks close to tens of parsec scales. Since local Seyfert galaxies have mass accretion rates of $\sim 0.01 M_{\odot} \text{ yr}^{-1}$ (Peterson 1997), it seems plausible that the analysis of Maciejewski (2004b) may be in the right direction. Further in the case of flocculent and tightly-sound nuclear spirals, it is not clear at present if the inflow rates are substantially reduced as compared to those in grand-design nuclear spirals, as detailed simulations have not been done.

The presence of strong shocks in the ISM is accompanied by star-formation activity. We noted in the previous section that we see more nuclear rings in NLS1’s as compared to BLS1’s, and the same is true for a barred *vs.* unbarred comparison. Presence of these bright stellar nuclear rings indicates that the central kiloparsec has been fueled in the last few hundred megayears. Further, bright star-forming regions are often seen on the outer periphery of the main curving dust lanes in these systems. Studies of the ring phenomena in galaxies, have shown that rings are resonance phenomena and are often found in galaxies with a large-scale bar, (Buta & Combes 1996). The size of nuclear rings in our sample corresponds with typical values for nuclear rings measured by other observers (Laine *et al.* 2002; Erwin & Sparke 2002; Martini *et al.* 2003a), and ranges from about 250 pc to 1 kpc; TOL 2327-027 would be an exception due to its large (≈ 5 kpc) circumnuclear disk (see Appendix). Laine *et al.* (2002) mention that size distribution of nuclear rings peaks at about the same radius as the location of the ILR of the main large-scale bar.

On the whole, we conclude that large-scale stellar bars drive the formation of and maintain grand-design nuclear dust spirals, which plausibly provide sufficient inflow rates to

fuel the SMBHs in NLS1’s. Recent simulations and the presence of star formation confined in a nuclear ring in the central kiloparsec give support to the idea that the gas loses its angular momentum via nuclear spiral shocks driven by the main bar potential. However, it is not clear what the mass inflow rates in flocculent nuclear spirals are. Since flocculent spirals are not driven by orbital resonances of a non-axisymmetric gravitational potential like a bar, it is plausible to expect that spiral shocks in flocculent spirals are much weaker, leading to less efficient accretion rates. Observational support for this is that very little star formation is seen in flocculent type nuclear spirals in unbarred galaxies, while grand-design spirals show enhanced star formation on the outer edges of their spiral arms and in stellar nuclear rings (Martini *et al.* 2003a, see also appendix in this paper). However inflow rates in flocculent spiral need to be studied using numerical simulations.

5. Conclusions

We have analyzed *HST* broad-band (F606W) images of a sample of 91 Seyfert 1 galaxies to study their nuclear morphology. We employed structure maps to enhance fine dust structure in the nuclear regions. Accompanying images in Figure 2 provide a good repository to study nuclear dust structures in Seyfert 1 galaxies.

Our sample contains 12 NLS1 hosts and 75 BLS1 host galaxies. This allowed us to compare the nuclear morphology of NLS1 host galaxies to the BLS1 host galaxies. In Crenshaw, Kraemer & Gabel (2003) (CKG03), we had noticed that NLS1’s showed more large-scale bars as compared to BLS1’s. We have revised the main morphological classification from CKG03 with the aid of structure maps, and conclude that 76% of NLS1 host galaxies are barred as compared to 40% for BLS1 hosts. Overall, almost half (47%) of the spiral Seyfert 1 galaxies from CKG03 are barred.

In this paper, we find that nuclear dust spirals are the most common kind of morphology in the central kiloparsec of Seyfert 1 galaxies. We find that 80% of the NLS1’s have grand-design type nuclear spirals as compared to 32% for BLS1’s. Further we see that 69% of barred galaxies have grand-design morphology as compared to 7% for unbarred ones. This is in agreement with the trend noted by Martini *et al.* (2003b). This is also indicative of the fact that these nuclear spirals are being driven and maintained by large-scale stellar bars. We also find that most BLS1 host galaxies have multi-arm, flocculent or chaotic nuclear dust spirals.

We find that 42% of the NLS1’s have nuclear star formation in the form of nuclear rings as compared to 11% of BLS1’s. Similar distribution is seen when one compares barred

galaxies with the unbarred ones. This again indicates that the large-scale bar is the main driver of these differences. This strengthens the idea that large-scale bars are important to support high fueling rates in NLS1's. Thus our results in this paper support the fueling scenario for barred *vs.* unbarred galaxies via nuclear dust spirals. Recent simulations of gas and dust inflow in barred galaxies give support to the idea that the galactic disk gas loses its angular momentum via nuclear spiral shocks which are being driven by the main bar potential within the central kiloparsec.

This research has made use of the NASA/IPAC Extragalactic Database (NED) which is operated by the Jet Propulsion Laboratory, California Institute of Technology, under contract with the National Aeronautics and Space Administration. This research has also made use of NASA's Astrophysics Data System Abstract Service. The data presented in this paper were obtained from the Multi-mission Archive at the Space Telescope Science Institute (MAST). Support for MAST for non-HST data is provided by the NASA Office of Space Science via grant NAG5-7584 and by other grants and contracts. We would also like to thank Dr. Buta for electronic access to The de Vaucouleurs Atlas of Galaxies.

APPENDIX

Notes on Individual Objects

Here we provide details on why we chose a particular classification for each galaxy. We also note the various dust features seen and any other special comments specific to each galaxy. Some of the galaxies show star-forming regions/stellar clusters in the circumnuclear region, these appear as small dark globular regions in the value-inverted images and often are associated with the dusty regions in the galaxy. Common sites for star formation seem to be dust lanes along the large-scale bars and in multi-arm loosely-wound spirals. In case of grand-design spirals most of the star-formation seems to be restricted to the outer edges of the dust lanes curving in to form the spiral. Often these form stellar nuclear rings. Many nuclear rings however seem to be associated with the “loosely-wound” type of nuclear spirals. We feel this is an important differentiator and may be indicative of evolution of nuclear regions of these galaxies. Galaxies with point source as the primary morphology classification do not have structure maps included in Figure 2 (see Malkan *et al.* (1998) for original images).

ESO 215-G14 (SB:DS:GD, BLS1) This galaxy has a noticeable bar in the structure map, but was originally classified as S (unbarred spiral) in CKG03. The bar is along approximately the east-west direction. Two very faint dust lanes are seen on leading edges of the bar. The structure map reveals a GD dust spiral in the center. Northern arm of the spiral is more clearly visible. The bar structure can be brought out by using a PSF with different size scale, here we chose the one that showed the inner spiral in clearest detail.

ESO 323-G77 (SB:DS:FL, BLS1, NR) Shows a multi-arm flocculent nuclear spiral along with a nuclear ring of star-burst regions encircling the spiral. Multiple large-scale dust lanes connect with the nuclear spiral at the position of the ring. Originally classified as a S (unbarred spiral) in CKG03.

ESO 354-G4 (S:DS:FL, BLS1) Shows filamentary multi-arm spiral structure on kiloparsec scale. Toward the center, nuclear spiral structure is smooth and has distinct puffy gaseous arms with small dust lanes embedded in them. The nuclear spiral is much smoother than the filamentary nature of the outer spiral. Spiral arms on north-west side are more distinct.

ESO 362-G18 (S:DS:FL, BLS1) Shows dust spiral structure in the inner kpc. Half of the galaxy is in the PC chip while the other half in WF2. Mosaic image shows star forming regions interspersed with dusty lanes. On the WF2 side a large-scale dust lane curves in toward the nucleus.

ESO 438-G9 (SB:DS:GD, BLS1) Large-scale dust lanes are apparent in main spiral arms as well as along the leading-edges of the bar. Prominent star forming regions are seen along the bar edges. Toward the center, the dust lanes curve in to form a grand-design type spiral. The inner regions of the nuclear spiral itself are lost in the bright saturated core. Both the

central kiloparsec as well as the bar structure shows chaotic dusty regions. Another galaxy similar to this one is MARK 766.

F 51 (SB:DS:?, BLS1) This galaxy is highly inclined, with large-scale dust lanes visible. The central kiloparsec shows chaotic dust structure along with bright emission to the west and south-west of the nucleus. Star-forming regions are seen at $\sim 7\text{--}8''$ from the galaxy center, which may be the outer co-rotation radius of the bar. It is not clear if the galaxy has a bar or a warped disk or if this is just an inclination effect.

F 1146 (S:DL:-, BLS1) This galaxy is too distant from us to resolve any nuclear features. But it has a large dusty disk (≈ 8 kpc) that is partially blocking the central AGN.

HEAO 1-0307-730 (SB:ND:-, BLS1) A prototype barred galaxy with two distinct spiral arms. It is again too distant to resolve nuclear structures. However the central 2-3 kpc look devoid of dust.

HEAO 1143-181 (I:A:?, BLS1) An Irregular galaxy, with emission line gas filaments visible, however it is too distant to resolve nuclear regions.

HEAO 2106-098 (P:ND:-, BLS1) Classified in CKG03 as a point source, it seems this galaxy is probably a SB type, the bar is noticeable in the structure map. However the galaxy is too distant to see any nuclear structure.

IC 1816 (SB:DS:?, BLS1) This one shows spectacular dust morphology on all scales. We see a nuclear dust spiral with two distinct arms that seem to open as the spiral travels inward eventually forming what looks like a bar-like structure. Curving dust lanes are prominent. This nuclear spiral has two distinct arms but is not the prototype GD, hence we have chosen to not include it in the GD category. The dust structure in the inner 500 pc along the north-south direction looks very similar to a gaseous/dust bar.

IC 4218 (S:DL:-, BLS1) Prominent dust lanes are seen in the main galactic disk. However, the inner 1-2 kpc are devoid of dust and are smooth. A single dust lane is seen all the way to the nucleus on the west side of the galactic disk. There is a hint of spiral (main) dust inflow along the inner side of this dust lane. Overall the galaxy is quite inclined.

IC 4329A (S:DL:-, BLS1) This is an edge-on galaxy with a large dust lane crossing the line of sight to the central source. No nuclear structures are visible.

IR 1249-131 (NGC 4748) (S:DS:GD, NLS1, NR) The large-scale structure shows a faint stellar bar extending from NE to SW. A curving dust lane from the NE side merges with the nuclear ring within the central $1\text{--}2''$. Inside the nuclear star-burst ring, a two arm nuclear dust spiral can be seen. The structure of the nuclear region is very similar to that of IC 1816, but we see a star-burst ring at about the same radius as the dust spiral arms. The star forming regions and/or emission regions are on the inside edges of the dust lanes. Much of

the rest of the central region seems to be chaotic. We chose to give it a GD classification as the dust lanes merge with fainter dust lanes along the large-scale bar.

IR 1319-164 (S:-:-, BLS1) This galaxy was excluded from analysis as most of it is outside the PC chip on the sawtooth side of WFPC/2 field of view.

IR 1333-340 (S:DL:-, BLS1) This one shows strong dust content within the central kiloparsec. However it is not clear if there is any spiral structure, hence we classify this as a DL for dust lane.

MCG 6-26-12 (SB:DS:GD, NLS1) This is a typical SB galaxy. Even though the central nuclear region is unresolved, we see curving dust lanes close to the central saturated core, that connect to the straight dust lanes along the leading-edges of the large-scale bar. Hence this is classified as a GD.

MCG 8-11-11 (SB:DS:?, BLS1) This galaxy was classified as a S in CKG03 but is a SB. One can clearly see a dust lane approaching the nucleus on the north side, eventually curving to the inner nuclear regions. Since we do not see the second dust lane on the opposite side of the bar, we haven't given it a GD classification.

MARK 6 (S:DL:-, BLS1) A strong dust lane passes close to the nucleus, much of the rest of the galaxy shows little dust structure.

MARK 10 (S:ND:-, BLS1) Very little dust is noticeable in the inner kiloparsec. The morphology is similar to IC 4218.

MARK 40 (? :ND:-, BLS1) This shows very little dust content in the nucleus, and seems to be an interacting system with a tidal tail. (Not displayed in Figure 2.)

MARK 42 (SB:DS:GD, NLS1, NR) A prototype barred galaxy with grand-design nuclear spiral and a star-burst nuclear ring. Curving dust lanes can be traced for slightly more than π radians.

MARK 50 (S:DS:FL, BLS1) Outer multi-arm spiral structure is too faint compared to the central source, but is seen in the structure map. This galaxy probably hosts a flocculent nuclear spiral. There is not much dust content visible close to the nucleus. There are hints of winding dust lane features within $1''$ of the nucleus.

MARK 79 (SB:DS:GD, BLS1) Two dust lanes along leading edges of the large-scale bar, curving toward the nucleus are seen. Nuclear structure is not prominent, mostly emission line gas filaments are visible.

MARK 279 (S:DS:FL, BLS1) Multi-arm flocculent nuclear spiral structure is visible. More dust structures are clearly visible on NW side of the nucleus.

MARK 290 (E:ND:-, BLS1) No significant dust in the nuclear region is visible. Mistakenly written as a unbarred spiral in CKG03, this galaxy is probably elliptical.

MARK 334 (S:DS:?, BLS1, SBS) Chaotic dust structures are seen on all scales. The central kiloparsec shows a distinct inverted S shaped spiral. The region connecting the two arms may also be interpreted as a dust bar. This galaxy may host a weak large-scale bar approximately along NE-SW line. Much of the nuclear spiral probably hosts sites of star formation. The spiral arms are relatively bright compared to other nuclear spirals.

MARK 335 (PG 0003+199) (P:-:-, NLS1) This galaxy is like a point source, no nuclear structure can be discerned.

MARK 352 (E:ND:-, BLS1) We see no significant dust in the nuclear region.

MARK 359 (SB:DS:GD, NLS1) Shows a very chaotic gaseous and dusty large-scale bar. The dust lanes are not as straight and clearly demarcated.

MARK 372 (S:DS:FL, BLS1) Shows a prototypical flocculent multi-arm nuclear dust spiral very similar to galaxies from class TW of Martini *et al.* (2003a)

MARK 382 (SB:DS:?, NLS1) Probably hosts a GD dust spiral, but central source is too bright to see it clearly. A curving dust lane NW of nucleus, along leading-edge of the large-scale bar is seen. We choose to not give it a secondary classification.

MARK 423 (S:DS:FL, BLS1) This galaxy is probably merging with its edge-on companion and shows a curious mirror-inverted “?” like view. There is extensive star-formation going on in the disk of the galaxy along with a disturbed dust morphology. We see chaotic gas structures with dust lanes in the central kiloparsec. A distinct two arm structure connected by a dust lane passes through the nucleus.

MARK 471 (SB:DS:GD, BLS1) We see chaotic dust structures within the large-scale bar. These dust lanes connect together and eventually curve toward the center to form a GD type structure. Dust can be traced all the way down to about 0.2'' of the nucleus.

MARK 493 (SB:DS:GD, NLS1, NR) Another prototypical galaxy with strong large-scale bar with leading-edge dust lanes feeding a central nuclear ring and a grand-design spiral toward the center. Also notable in this image is the presence of multiple dust spiral arms outside the nuclear ring. The nuclear ring is broken in places where these dust spiral arms connect with inner structure. These arms probably are the four-armed spiral outside the outer ILR of the large-scale bar (see, Maciejewski 2004b).

MARK 516 (S:DS:FL, BLS1) We see that the nuclear dust morphology is chaotic and extensive star-formation is going on. The nuclear region shows two bright nuclei.

MARK 530 (S:DS:FL, BLS1, NR) This galaxy shows dust content on all scales, the nuclear spiral has multiple dust arms and is of flocculent (FL) type. To the SW of the nucleus just on the outer edge of the curving dust arm, a star-burst region is prominent.

MARK 543 (S:DS:FL, BLS1) Shows dust on large scales. Multiple spiral arms littered with star forming regions are seen. However the central 1-2 kpc appear to be smooth and devoid of dust.

MARK 590 (S:DS:FL, BLS1) This galaxy is similar to MARK 543, but this time the central regions are much more clearly visible. One can see multiple dust spiral arms intermingled with puffy-looking smooth emission. It is at about the same distance as MARK 543, but the star forming regions and multiple dust arms are located on the outer edges of the galactic disk as compared to MARK 543.

MARK 595 (S:DS:FL, BLS1) Shows a multi-arm flocculent dust spiral. One also sees a nuclear emission ring-like structure close to the central source crossed by a straight dust lane, which connects on one side with a dusty spiral arm. Spiral pattern north of the nucleus is not seen.

MARK 609 (S:DS:FL, BLS1) Shows multiple dust spiral arms on all scales. The overall look is that of a chaotic spiral.

MARK 699 (E:ND:-, NLS1) This galaxy is like a point source and almost no structure is visible.

MARK 704 (SB:A:?, BLS1) This is a SB galaxy with very little dust structure visible due to the bright nucleus, however there is dust structure that appears to be curving dust lanes just near the point source.

MARK 744 (S:DS:?, BLS1, NR) This galaxy shows a dusty and gaseous nuclear spiral, large dust lanes are seen on Northern side of the galactic disk. Central spiral has multiple dusty arms that wind by more than 2π . A nuclear ring may be forming at about $1''$ distance from the nucleus.

MARK 766 (SB:DS:GD, NLS1) This is a prototype barred NLS1 with large amount of dust in the large-scale bar along with the curving dust lanes toward the center, that eventually form a grand-design type of nuclear spiral.

MARK 817 (SB:DS:GD, BLS1) Another prototypical barred galaxy with leading-edge dust lanes culminating in grand-design nuclear spiral.

MARK 833 (I:A:?, BLS1) This is an irregular galaxy with a hint of formation of spiral structure and a bar along its NW direction. The dust structure is mostly amorphous.

MARK 871 (S:DL:-, BLS1) This is a spiral galaxy with large dust lanes and a smooth inner disk. A large dust lane is traveling all the way to the central source on the NW side of

nucleus. Similar dust lane is absent on the SE side, however dust lanes seem to be curving toward the nucleus, about $6.5''$ from the nucleus.

MARK 885 (SB:DS:GD, BLS1) This is a barred galaxy, with leading-edge dust lanes along the bar. However they do not form a typical GD structure in the central kiloparsec. The dust lanes south of the nucleus seems to merge partly with a dust lane from the other side of the bar on the NE side of the nucleus. The curved dust structure on the north side of the nucleus extends till it merges toward the nucleus.

MARK 896 (SB:DS:GD, NLS1, NR) This is another prototype barred galaxy showing grand-design nuclear spiral with a nuclear ring. Originally classified as a S (unbarred spiral) in CKG03.

MARK 915 (S:DS:GD, BLS1) This is a spectacular example of a dust lane tracing all the way to the nucleus. The galaxy also shows cone-shaped NLR emission regions which are almost perpendicular to the inflowing dust structures. The galaxy is highly inclined.

MARK 1040 (S:DL:-, NLS1) Another spectacular example of a large-scale dust lane obscuring the central regions. Not much can be inferred from the nuclear regions.

MARK 1044 (SB:DS:FL, NLS1, SBS) This is a interesting galaxy showing large-scale dust lanes along leading-edges of the main bar, feeding what looks like a multi-arm flocculent type spiral. However the dust lanes can be traced for about 2π radians before they disappear in the central saturated PSF core. The multi-arm stellar spiral could be the four-armed spiral that forms at the outer ILR. Originally classified as a S (unbarred spiral) in CKG03.

MARK 1126 (SB:DS:GD, BLS1) This is another prototype barred galaxy with a distinct grand-design nuclear dust spiral in the center. The inner extension of the spiral may be interpreted as a dust bar. However the change in pitch angle of the spiral is quite strong and it seems similar change on the west side of nucleus is being masked by the strong emission from the nucleus in that direction. Originally classified as a S (unbarred spiral) in CKG03.

MARK 1218 (SB:DS:GD, BLS1) This is a flocculent spiral that is being fed by large-scale dust lanes. In the nuclear regions, the dust structure is mostly chaotic. The galaxy is probably barred.

MARK 1330 (SB:DS:GD, BLS1) Shows a gaseous and dusty nuclear spiral. The single spiral arm is spectacular and traveling all the way to the nucleus, where the flow seems to disintegrate in to chaotic gas and dust clouds. We earlier classified it as a FL based only on the PC image, but after looking at the mosaic image one can see that the dust extensions on the north and south side of the nuclear spiral connect to the dust lanes on leading edges of the large-scale bar. Hence we reclassified it as a GD. Originally classified as a S (unbarred spiral) in CKG03.

MARK 1376 (S:DL:-, BLS1) This galaxy is highly inclined and hence it is impossible to see the nuclear dust structure. An ionization cone like structure is emanating from the nucleus almost perpendicular to the dust lanes. Originally not classified (category ?) in CKG03.

MARK 1400 (S:DS:?, BLS1) The central structure of MARK 1400 is smooth and very little dust structure is seen. There is hint of a dust spiral in the central 2-3 kpc.

MARK 1469 (S:DL:-, BLS1) This galaxy is highly inclined with only large-scale dust lanes visible.

MS 1110+2210 (E:ND:-, BLS1) This galaxy is completely featureless, with no detectable dust structure close to the nucleus.

NGC 235 (S:DS:FL, BLS1) This galaxy shows a flocculent tightly winding nuclear dust spiral.

NGC 526A (I:DL:-, BLS1) This is peculiar galaxy with a large veil-like dust structure in front of the central nucleus. We classified this as a dust lane type (DL).

NGC 1019 (SB:DS:GD, BLS1, NR) This is a spectacular galaxy showing two large-scale spiral arms with dust lanes, a large-scale bar with leading-edge dust lanes, a distinct nuclear star-forming ring at about 1 kpc from the nucleus. There is a dust lane traveling all the way to the nucleus from the SE side inside the nuclear ring. The inner disk appears featureless and mostly devoid of dust except for the faint dust lanes visible on North and SE of the nucleus. The SE lane connects with curving dust lane of the northern arm of the large-scale bar. Faint multi-arm spiral extensions are seen around the nuclear ring, these are probably similar to the four-armed type spiral patterns seen in other barred galaxies with an outer ILR.

NGC 1566 (S:DS:FL, BLS1) This is a Sbc galaxy having a flocculent dusty nuclear spiral. Very close to the nucleus the spiral shows a curious inverted S shaped structure in the inner 1".

NGC 2639 (S:DS:FL, BLS1) This is a spectacular galaxy showing multi-arm flocculent dust spiral structure on large-scales. In the inner 5" from the nucleus the disk becomes much smoother with two dust lanes traveling toward the nucleus. The puffy nuclear gas disk probably has 3 or 4 spiral arms.

NGC 3227 (SB:DL:-, BLS1) The inner disk is highly inclined and hence we can only see dust lanes crossing it on the SW side. Looking at the WFPC2 mosaic image, these dust lanes are the inner parts of the leading-edge dust lanes of the large-scale bar. The dust within the large-scale bar is also chaotic. We are not seeing the other edge of the bar on the SE side in the WFPC2 image. Emission line gas is seen near the nucleus and perpendicular to the disk plane. Since we cannot see the nuclear structure clearly, we choose to classify this as a DL. Originally not classified (category ?) in CKG03.

NGC 3516 (SB:DL:-, BLS1) This is a spiral galaxy with a large chaotic dust lane traveling toward the nucleus. There are more dusty regions south of the nucleus. The large-scale structure is not clearly seen, but it seems like the galaxy is a SB type in the WFPC1 mosaic image, and the bar may lie on NW-SE line with respect to the nucleus. It is unclear what is generating the large-scale chaotic dust lane. Originally classified as a S (unbarred spiral) in CKG03.

NGC 3783 (SB:DS:FL, BLS1) This is a typical barred galaxy, with a large-scale star+dust ring at outer co-rotational radius of the bar. The dust lanes along the bar edges are faint. We can see curving dust lanes from the bar edges, but apart from that there are multiple dust lanes, so we choose to go with the FL category for this galaxy.

NGC 4051 (SB:DS:GD, NLS1) This shows a gas and dust rich nuclear region. We choose to classify this galaxy as a GD based on the dust lane NE of the nucleus which connects to the large-scale leading-edge dust lane of the bar. This is not immediately apparent from the PC image due to proximity of the galaxy.

NGC 4235 (S:DL:-, BLS1) This galaxy is highly inclined and we only see the large-scale dust lane.

NGC 5252 (S:DS:?, BLS1) This is a curious galaxy with dust filaments stretching in arcs all the way out to 15'' and a stellar bar like structure which is completely devoid of dust, stretching along the NS line. One sees a tightly wounding spiral structure NW of the nucleus. Since we could not properly classify this we chose to only give it the primary classification of DS.

NGC 5548 (S:DS:FL, BLS1) This one shows a inwardly winding nuclear dust spiral. The overall morphology is similar to NGC 7213.

NGC 5674 (SB:DS:GD, BLS1) This is a prototype barred spiral with spectacular grand-design nuclear spiral. Dust content is seen on all scales.

NGC 5940 (SB:DS:GD, BLS1) This is another barred spiral with a spectacular grand-design nuclear spiral. Dust content is again prominent on all scales.

NGC 6104 (SB:DS:?, BLS1) Dust content is prominent on all scales. A strong large-scale bar is visible, but only one leading-edge dust lane is visible on the NE side of the nucleus. This lane curves and moves toward the nucleus, however since we do not see the other lane we choose to not give it a secondary classification. This is probably a GD.

NGC 6212 (S:DS:FL, BLS1, NR) This is a spectacular example of a multi-arm flocculent spiral structure for the outer disk and a tightly wound multi-arm structure for the nuclear disk. This is what would be a prototype class TW nuclear spiral from the classification of Martini *et al.* (2003a). It also shows a nuclear star-forming ring at between 2 and 3'' from the nucleus.

NGC 6860 (S:DS:FL, BLS1) This galaxy is partly out of the PC chip, but one can see the dust lanes that connect the outer dusty disk with the nucleus. Most of the nuclear disk is smooth.

NGC 7213 (S:DS:FL, BLS1) This a prototype galaxy for a multi-arm flocculent inwardly winding nuclear dust spiral. The dust spiral can be traced all the way to the nucleus. The nuclear disk is packed with large quantities of gas and dust.

NGC 7314 (S:DS:FL, BLS1) The inclined nuclear disk shows chaotic dust content and hence is classified as FL.

NGC 7469 (S:DS:?, BLS1, NR) Shows a good example of a multi-arm nuclear spiral with a nuclear star-burst ring.

II SZ 10 (S:ND:-, BLS1) This is a barred spiral but is too distant to search for nuclear structures. This was mistakenly written as II ZW 10 in CKG03 as the MAST fits header gives 'IIZW10' as the value of 'TARGNAME' parameter.

PKS 0518-458 (E:ND:-, BLS1) This is a elliptical galaxy but too distant to look for nuclear structures.

TOL 1059+105 (S:ND:-, BLS1) This galaxy has bright emission line filaments near its nucleus, but shows no dust content.

TOL 2327-027 (SB:DS:GD, BLS1, NR) This is a spectacular example of a nuclear grand-design spiral. It can be questioned if we can call the spiral that starts at ≈ 5 kpc a nuclear spiral. We can trace winding dust lanes all the way down to 200 pc from the nucleus. At about ≈ 2 kpc the winding of large dust lanes halts and the galaxy seems to have formed a gaseous disk; small dust lanes continue through this disk toward the nucleus. All the star forming regions seem to form in a ring-like structure and are on the outer side of the curving dust lanes. Originally classified as a S (unbarred spiral) in CKG03.

UM 146 (S:DS:?, BLS1) The dust structure in this galaxy is quite faint in the nucleus which is dominated by the optical emission of the nuclear gas disk. One can see small dust lanes crossing the disk. It is possible that the disk is being fueled via large-scale dust lanes, but these are not clearly visible, except on the east side of the nucleus.

UGC 3223 (SB:DS:FL, BLS1) This one shows a flocculent multi-arm disk in the nuclear region. Dust is distributed on large scale in the galaxy and one can see a dust lane traveling toward the nucleus from the north side of the galaxy. This dust lane eventually curves to become the nuclear spiral. There is a ring-like structure around the nucleus. Originally classified as a S (unbarred spiral) in CKG03.

WAS45 (SB:DS:GD, BLS1, NR) This galaxy probably has a grand-design nuclear spiral and is similar in morphology to MARK 1044. A nuclear stellar ring is clearly visible.

UGC 10683B (SB:DS:?, BLS1) This one shows a dusty tightly wound nuclear spiral.

UGC 12138 (SB:DS:GD, BLS1) This one shows a grand-design nuclear dust spiral. The bar is probably not strong as the leading-edge dust lanes are not straight lines but curved.

UM 614 (S:ND:-, BLS1) Very little dust is seen in the nuclear regions of this galaxy.

X 0459+034 (E:A:-, BLS1) This galaxy shows extended emission line gas filaments but no dust structure is detectable in nuclear region.

REFERENCES

- Adams, T. 1977, ApJS, 33, 19
- Boroson, T.A. & Green, R. F. 1992, ApJS, 80, 109
- Buta, R. & Combes, F. 1996, Fund. Cosmic Physics, Vol. 17, 95
- Crenshaw, D. M., Kraemer, S. B. & Gabel, J. R. 2003, AJ, 126, 1690 (CKG03)
- De Robertis, M. M., Yee, H. K. C., & Hayhoe, K. 1998, ApJ, 496, 93
- de Vaucouleurs, G. *et al.* 1991, Third Reference Catalogue of Bright Galaxies (New York: Springer)
- Englmaier, P. & Shlosman, I. 2000, ApJ, 528, 677
- Erwin, P. & Sparke, L. S. 2002, AJ, 124, 65
- Erwin, P. & Sparke, L. S. 2003, ApJS, 146, 299
- Goldreich, P., & Tremaine, S. 1978, ApJ, 222, 850
- Goldreich, P., & Tremaine, S. 1979, ApJ, 233, 857
- Goodrich, R. W., 1989, ApJ, 342, 234
- Heckman, T. M. 1980, A&A, 88, 365
- Ho, L. C., Filippenko, A. V., & Sargent, W. L. W. 1997, ApJ, 487, 591
- Jogee, S., Shlosman, I., Laine, S., Englmaier, P., Knapen, J. H., Scoville, N., & Wilson, C. D. 2002, ApJ, 575, 156
- Khachikian, E. Ye. & Weedman, D. W. 1974, ApJ, 192, 581
- Kormendy, J. & Richstone, D. 1995, ARA&A, 33, 581
- Koski, A. 1978, ApJ, 223, 56
- Krist, J. E. & Hook, R. N. 1999, The Tiny Tim User's Guide (Baltimore: STScI)
- Laine, S., Shlosman I., Knapen, J. H. & Peletier, R. F. 2002, ApJ, 567, 97
- Maciejewski, W. 2004a, MNRAS, 354, 883
- Maciejewski, W. 2004b, MNRAS, 354, 892

- Maciejewski, W., Teuben, P. J., Sparke, L. S., & Stone, J. M. 2002, MNRAS, 329, 502
- Maiolino, R., Alonso-Herrero, A., Anders, S., Quillen, A., Rieke, M. J., Rieke, G. H., & Tacconi-Garman, L. E. 2000, ApJ, 531, 219
- Malkan, M. A., Gorjian, V. & Tam, R. 1998, ApJ, 117, 25
- Martini, P., Regan, M. W., Mulchaey, J. S., & Pogge, R. W. 2003a, ApJS, 146, 353
- Martini, P., Regan, M. W., Mulchaey, J. S., & Pogge, R. W. 2003b, ApJ, 589, 774
- Martini, P. & Pogge, R. W., 1999, AJ, 118, 2646
- Mathur, S., Kuraszkiewicz, J., & Czerny, B. 2001, NewA, 6, 321
- Miller, J. S., & Antonucci, R. R. J. 1983, ApJ, 271, L7
- Mulchaey, J. S., Regan, M. W., & Kundu, A. 1997, ApJS, 110, 299
- Mulchaey, J. S., & Regan, M. W. 1997, ApJ, 482, L135
- Osterbrock, D. E., & Pogge, R. W. 1985, ApJ, 297, 166
- Osterbrock, D. E. 1977, ApJ, 215, 733
- Osterbrock, D. E. 1981, ApJ, 249, 462
- Patsis, P. A. & Athanassoula, E. 2000, A&A, 358, 45
- Peterson, B. M. 1997, An Introduction to Active Galactic Nuclei, Cambridge University Press, Cambridge, UK
- Peterson, B. M. *et al.* 2004, ApJ, 613, 682
- Pogge, R. W. & Martini, P. 2002, ApJ, 569, 624
- Pounds, K. A., Done, C. & Osborne, J. P. 1995, MNRAS, 277, L5
- Regan, M. W., & Mulchaey, J. S. 1999, AJ, 117, 2676
- Schmidt, M. & Green, R. F. 1983, ApJ, 269, 352
- Seyfert, C. K., 1943, ApJ, 97, 28
- Shlosman, I., Begelman, M. C., & Frank, J. 1990, Nature, 345, 679
- Simkin, S. M., Su, H. J., & Schwarz, M. P. 1980, ApJ, 237, 404

Spergel, D. N., et al. 2003, ApJS, 148, 175

Toomre, A., & Toomre, J. 1972, ApJ, 178, 623

Véron-Cetty, M., -P., & Véron, P. 2001, A&A, 374, 92

Wandel, A. 2002, ApJ, 565, 762

Fig. 1.— Host Galaxy Properties of the Sample: Histograms of four host galaxy parameters: the redshift (z), the galaxy inclination (i) in degrees, numerical Hubble stage index (T) and the absolute blue magnitude (M_B^0) for the NLS1 (shaded histogram) *vs.* BLS1 sample.

Fig. 2.— Structure maps of *HST* WFPC2 images of Seyferts 1s in Table 1: All images are archival F606W snapshots. Images shown in this paper are structure maps (see Malkan *et al.* (1998) for original images). Rows one and three show a 600 x 600 pixel region of the PC chip to avoid overscan regions. Rows two and four show the same image, but zoomed to show the nuclear structure. See the scale on the left side of plots for exact dimensions in arcsecond. All images are color inverted. Dust structures are white and bright emission regions are dark.

Fig. 3.— Frequency of Nuclear Dust Structures: Figure shows bar plots for various morphological classes shown in Table 3. See §2.2 in text for description of morphology classes. Plots on the right side compare barred galaxies against unbarred ones. Plots on the left side compare NLS1’s with BLS1’s. Plots on the top row pertain to the primary nuclear morphology classification, while plots on the bottom row pertain to the secondary classification within the DS class from the top row. In the top row plots, the dashed partition separates stellar nuclear rings from nuclear dust structures. The statistics for nuclear rings also includes two starburst nuclear spirals: MARK 334 and MARK 1044, for simplicity.

Table 1. Nuclear Morphology and Host Galaxy Parameters for Seyfert 1 Galaxies

Name	Redshift	b/a^h	Hubble ^h Stage	M_B^{0h}	Seyfert 1 Class	Large-scale Morph.	Nuclear Morph.
(1)	(2)	(3)	(4)	(5)	(6)	(7)	(8)
ESO 215-G14	0.019	0.70	3.0		BLS1	SB	DS (GD)
ESO 323-G77	0.015	0.67	-2.2	-20.92	BLS1	SB	DS (FL), NR
ESO 354-G4	0.033	0.82	2.7	-21.53	BLS1	S	DS (FL)
ESO 362-G18	0.013	0.67	-0.3	-20.12	BLS1	S	DS (FL)
ESO 438-G9	0.024	0.70	2.2	-21.41	BLS1	SB	DS (GD)
F 51	0.014	0.56	2.8	-20.20	BLS1	SB	DS (?)
F 1146 ^b	0.032	0.62	3.0		BLS1	S	DL
HEAO 1-0307-730	0.028	0.50	1.0		BLS1	SB	ND
HEAO 1143-181	0.033	0.88	90.0		BLS1	I	A
HEAO 2106-099 ^d	0.027	0.60	0.0		BLS1	P	ND
IC 1816	0.017	0.86	2.4	-20.62	BLS1	SB	DS (?)
IC 4218	0.019	0.23	1.0	-20.89	BLS1	S	DL
IC 4329A	0.016	0.29	-0.7	-20.51	BLS1	S	DL
IR 1249-131 ^f	0.014	0.58	3.0		NLS1	S	DS (GD), NR
IR 1319-164 ^e	0.017	0.80	3.0		BLS1	S	-
IR 1333-340	0.008	0.60	-2.0	-19.24	BLS1	S	DL
MCG 6-26-12	0.032	0.13	4.7		NLS1	SB	DS (GD)
MCG 8-11-11	0.020	0.71	1.0	-21.54	BLS1	SB	DS (?)
MARK 6	0.019	0.63	-0.5	-20.05	BLS1	S	DL
MARK 10	0.030	0.39	3.0	-22.62	BLS1	S	ND
MARK 40	0.020	0.43	-2.0		BLS1	?	ND
MARK 42	0.024	0.98	2.0	-20.00	NLS1	SB	DS (GD), NR
MARK 50	0.023	0.60	-2.0	-20.05	BLS1	S	DS (FL)
MARK 79	0.022	1.00	3.0	-21.52	BLS1	SB	DS (GD)
MARK 279	0.031	0.56	-2.0	-21.15	BLS1	S	DS (FL)
MARK 290	0.029	0.89	-5.0	-20.37	BLS1	E	ND
MARK 334	0.022	0.70	99.0	-20.83	BLS1	S	DS (?), SBS
MARK 335 ^d	0.025	1.00	0.0		NLS1	P	-
MARK 352	0.015	0.50	-2.0	-19.52	BLS1	E	ND
MARK 359	0.017	0.83	0.0	-20.44	NLS1	SB	DS (GD)
MARK 372	0.031	0.80	1.0	-21.23	BLS1	S	DS (FL)
MARK 382	0.034	0.92	4.0	-20.94	NLS1	SB	DS (?)
MARK 423	0.032	0.56	3.0	-21.01	BLS1	S	DS (FL)
MARK 471	0.034	0.67	1.0	-21.57	BLS1	SB	DS (GD)

Table 1—Continued

Name	Redshift	b/a^h	Hubble ^h Stage	M_B^{0h}	Seyfert 1 Class	Large-scale Morph.	Nuclear Morph.
(1)	(2)	(3)	(4)	(5)	(6)	(7)	(8)
MARK 493	0.031	0.83	3.0	-21.13	NLS1	SB	DS (GD), NR
MARK 516	0.028	0.83	4.0	-20.36	BLS1	S	DS (FL)
MARK 530	0.029	0.67	3.0	-21.84	BLS1	S	DS (FL), NR
MARK 543	0.026	1.00	6.0	-20.23	BLS1	S	DS (FL)
MARK 590	0.027	0.91	1.3	-21.61	BLS1	S	DS (FL)
MARK 595	0.028	0.68	1.0	-21.00	BLS1	S	DS (FL)
MARK 609	0.032	0.90	1.0		BLS1	S	DS (FL)
MARK 699 ^d	0.034	0.87	-4.0	-20.16	NLS1	E	ND
MARK 704	0.029	0.57	1.0	-20.55	BLS1	SB	A
MARK 744	0.010	0.59	1.0	-20.16	BLS1	S	DS (?), NR
MARK 766	0.012	0.80	1.0	-19.73	NLS1	SB	DS (GD)
MARK 817	0.033	1.00	4.0	-21.36	BLS1	SB	DS (GD)
MARK 833	0.039	0.75	90.0		BLS1	I	A
MARK 871	0.034	0.50	0.0	-21.29	BLS1	S	DL
MARK 885	0.026	0.57	3.0	-20.41	BLS1	SB	DS (GD)
MARK 896	0.027	0.73	3.0		NLS1	SB	DS (GD), NR
MARK 915	0.025	0.30	3.0		BLS1	S	DS (GD)
MARK 1040	0.016	0.21	4.0	-21.92	NLS1	S	DL
MARK 1044	0.016	0.86	1.0		NLS1	SB	DS (FL), SBS
MARK 1126	0.010	1.00	1.0		BLS1	SB	DS (GD)
MARK 1218	0.028	0.50	3.0	-20.83	BLS1	SB	DS (GD)
MARK 1330	0.009	0.74	3.0	-21.47	BLS1	SB	DS (GD)
MARK 1376	0.007	0.24	1.0	-20.09	BLS1	S	DL
MARK 1400	0.029	0.50	1.0		BLS1	S	DS (?)
MARK 1469	0.031	0.36	3.0		BLS1	S	DL
MS 1110+2210	0.030	0.86	-4.0		BLS1	E	ND
NGC 235	0.022	0.54	-2.0	-20.87	BLS1	S	DS (FL)
NGC 526A	0.018	0.53	-2.0		BLS1	I	DL
NGC 1019	0.024	0.90	3.5	-20.86	BLS1	SB	DS (GD), NR
NGC 1566	0.004	0.80	4.0	-20.98	BLS1	S	DS (FL)
NGC 2639	0.011	0.61	1.0	-21.14	BLS1	S	DS (FL)
NGC 3227	0.003	0.67	1.0	-19.33	BLS1	SB	DL
NGC 3516	0.009	0.77	-2.0	-20.76	BLS1	SB	DL
NGC 3783	0.009	0.89	1.5	-20.86	BLS1	SB	DS (FL)
NGC 4051	0.002	0.75	4.0	-18.89	NLS1	SB	DS (GD)

Table 1—Continued

Name	Redshift	b/a^h	Hubble ^h Stage	M_B^{0h}	Seyfert 1 Class	Large-scale Morph.	Nuclear Morph.
(1)	(2)	(3)	(4)	(5)	(6)	(7)	(8)
NGC 4235	0.007	0.21	1.0	-20.46	BLS1	S	DL
NGC 5252	0.022	0.56	-2.0	-20.91	BLS1	S	DS (?)
NGC 5548	0.017	0.93	0.0	-21.47	BLS1	S	DS (FL)
NGC 5674	0.025	0.91	5.0	-21.55	BLS1	SB	DS (GD)
NGC 5940	0.033	1.00	2.0	-21.60	BLS1	SB	DS (GD)
NGC 6104	0.028	0.82	3.0	-21.39	BLS1	SB	DS (?)
NGC 6212	0.030	0.76	3.0	-20.58	BLS1	S	DS (FL), NR
NGC 6860	0.015	0.62	2.6	-20.80	BLS1	S	DS (FL)
NGC 7213	0.006	0.90	1.0	-20.89	BLS1	S	DS (FL)
NGC 7314	0.006	0.46	4.0	-20.93	BLS1	S	DS (FL)
NGC 7469	0.017	0.73	1.0	-21.64	BLS1	S	DS (?), NR
II SZ 10 ^g	0.034	0.60	4.0		BLS1	S	ND
PKS 0518-458 ^c	0.034	0.69	-2.0	-19.84	BLS1	E	ND
TOL 1059+105	0.034	0.45	-1.0	-20.66	BLS1	S	ND
TOL 2327-027	0.033	0.68	2.7		BLS1	SB	DS (GD), NR
UM 146	0.017	0.77	3.0	-20.42	BLS1	S	DS (?)
UGC 3223	0.018	0.57	1.0	-21.32	BLS1	SB	DS (FL)
WAS 45 ^c	0.024	1.00	3.0	-20.92	BLS1	SB	DS (GD), NR
UGC 10683B	0.031	0.50	1.0		BLS1	SB	DS (?)
UGC 12138	0.025	0.88	1.0	-21.33	BLS1	SB	DS (GD)
UM 614 ^b	0.033	0.52	-1.0	-20.88	BLS1	S	ND
X 0459+034 ^a	0.016	0.82	-4.0		BLS1	E	A

Note. — All images except as noted were taken with F606W filter. Large-scale galactic morphology classes are; S: spiral, SB: barred spiral, E: elliptical, I: irregular, P: point source and ?: not classified. Primary nuclear morphology classes are; ND: no significant dust, DS: dust spiral, DB: dust bar, A: amorphous structures, DL: large-scale dust lane, NR: Nuclear Ring and SBS: Star-burst (nuclear) Spiral. Secondary nuclear morphology classes are; GD: grand-design spiral, FL: flocculent multi-arm spiral and ?: for no secondary classification.

^aObserved with the F814W filter.

^bGalaxy positioned in WF2 chip

^cGalaxy positioned in WF4 chip

^dNot included in Figure 2.

^eExcluded from analysis, see §2.1

^fOther name: NGC4748

^gThe MAST fits header entry for this galaxy mentions it as II ZW 10 which is incorrect.

^hData values were selected from NED for these columns. Some values for the Hubble stage T were reassigned using classifications from The de Vaucouleurs Atlas of Galaxies, Buta, Corwin and Odewahn (in preparation).

Table 2. Host Galaxy Properties of the Sample

Parameter	All (87)			NLS1 (12/87)			BLS1 (75/87)		
	Median	Mean	σ	Median	Mean	σ	Median	Mean	σ
Redshift (z)	0.024	0.022	0.01	0.024	0.022	0.01	0.024	0.023	0.01
Inclination i (deg.)	46.37	43.70	19.36	36.87	41.58	20.92	47.93	44.31	18.87
Hubble Stage (T)	1.0	1.3	2.3	3.0	2.1	2.4	1.0	1.2	2.3
M_B^0 (mag.)	-20.88	-20.80	0.69	-20.16	-20.40	0.93	-20.89	-20.86	0.64

Table 3. Frequency of Primary Nuclear Dust Structures^a

Galaxy Class	No Dust	Dust Spiral ^c	Dust Bar	Amorph.	Dust Lane	Nuclear ^d Ring
Seyfert 1s (87) ^b	0.11 (10 ± 3.0)	0.69 (60 ± 4.3)	0.00 (0)	0.05 (4 ± 2.0)	0.15 (13 ± 3.3)	0.16 (14 ± 3.4)
NLS1's (12)	0.08 (1 ± 1.0)	0.83 (10 ± 1.3)	0.00 (0)	0.00 (0)	0.08 (1 ± 1.0)	0.42 (5 ± 1.7)
BLS1's (75)	0.12 (9 ± 2.8)	0.67 (50 ± 4.1)	0.00 (0)	0.05 (4 ± 2.0)	0.16 (12 ± 3.2)	0.12 (9 ± 2.8)
Barred Spirals (36)	0.03 (1 ± 1.0)	0.89 (32 ± 1.9)	0.00 (0)	0.03 (1 ± 1.0)	0.06 (2 ± 1.4)	0.32 (8 ± 2.5)
Spirals (42)	0.10 (4 ± 1.9)	0.67 (28 ± 3.1)	0.00 (0)	0.00 (0)	0.24 (10 ± 2.8)	0.11 (6 ± 2.3)

^aGiven as fractions; number of galaxies in each group is given in parenthesis, along with binomial errors.

^bOut of a total of 91 Seyferts, 87 have both nuclear and large-scale morphological type defined.

^cDust spirals are further classified into Grand Design and Flocculent types, see Table 4.

^dThe nuclear ring category also includes the two nuclear spirals showing starburst spiral arms, MARK 334 and MARK 1044, for simplicity.

Table 4. Frequency of Nuclear Dust Spiral Morphology^a

Galaxy Class ^c	Nuclear Spiral Morphology		
	Grand Design ^b	Flocculent ^b	Undefined ^b
Seyfert 1s (60)	0.40 (24 ± 4.0)	0.40 (24 ± 3.8)	0.20 (12 ± 3.1)
NLS1's (10)	0.80 (8 ± 1.3)	0.10 (1 ± 1.0)	0.10 (1 ± 1.0)
BLS1's (50)	0.32 (16 ± 3.3)	0.46 (23 ± 3.5)	0.22 (11 ± 2.9)
Barred Spirals (32)	0.69 (22 ± 2.6)	0.12 (4 ± 1.9)	0.19 (6 ± 2.2)
Spirals (28)	0.07 (2 ± 1.4)	0.71 (20 ± 2.4)	0.21 (6 ± 2.2)

^aGiven as fractions; number of galaxies in each group is given in parenthesis, along with binomial errors.

^bNuclear spiral classification: these are galaxies that show dust spirals as their primary nuclear morphology.

^cThe numbers in parenthesis in this column come from column 3 in Table 3, *e.g.*, out of 87 Seyfert 1's in Table 3, 60 have dust spirals.

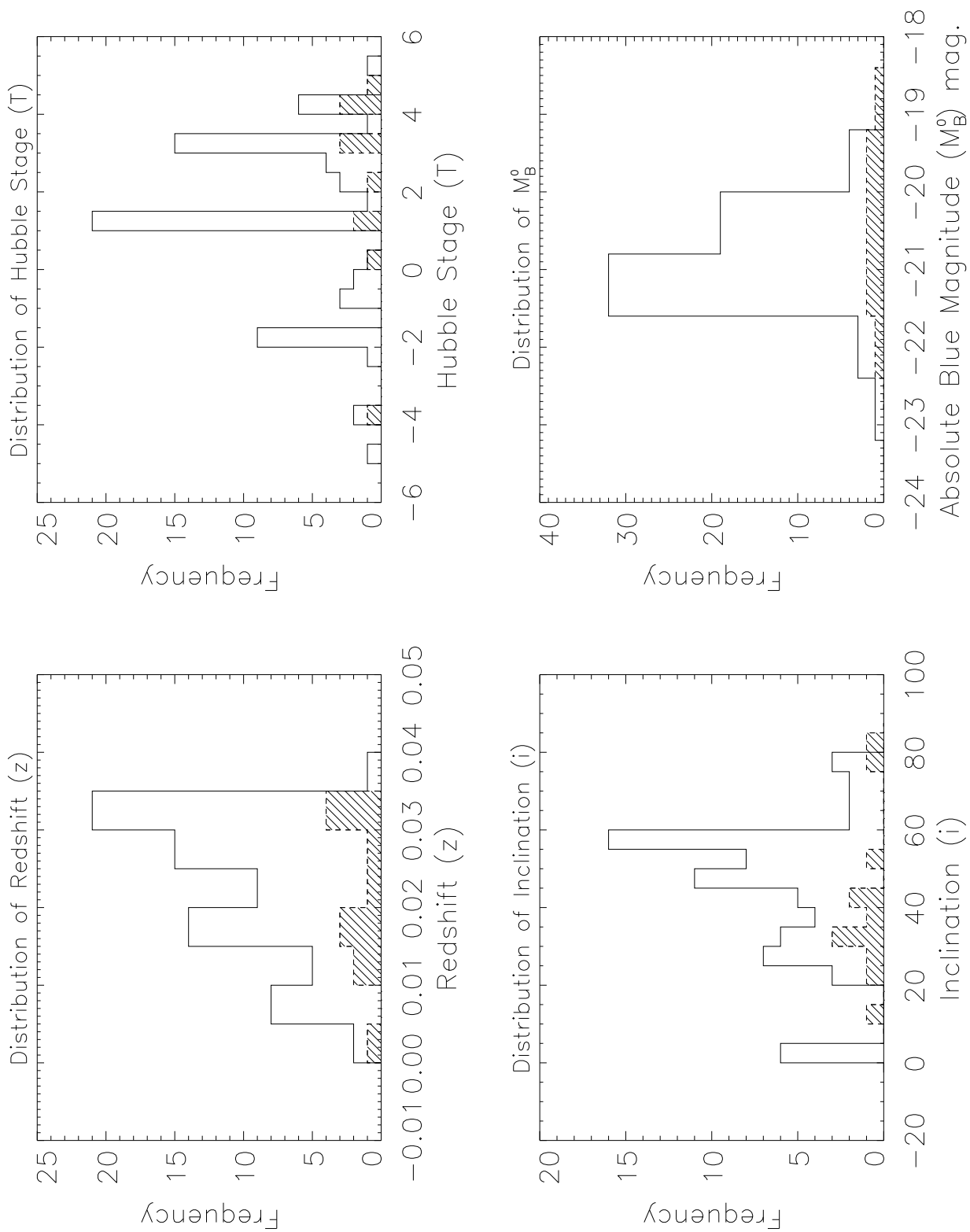


Fig. 1.— Host Galaxy Properties of the Sample

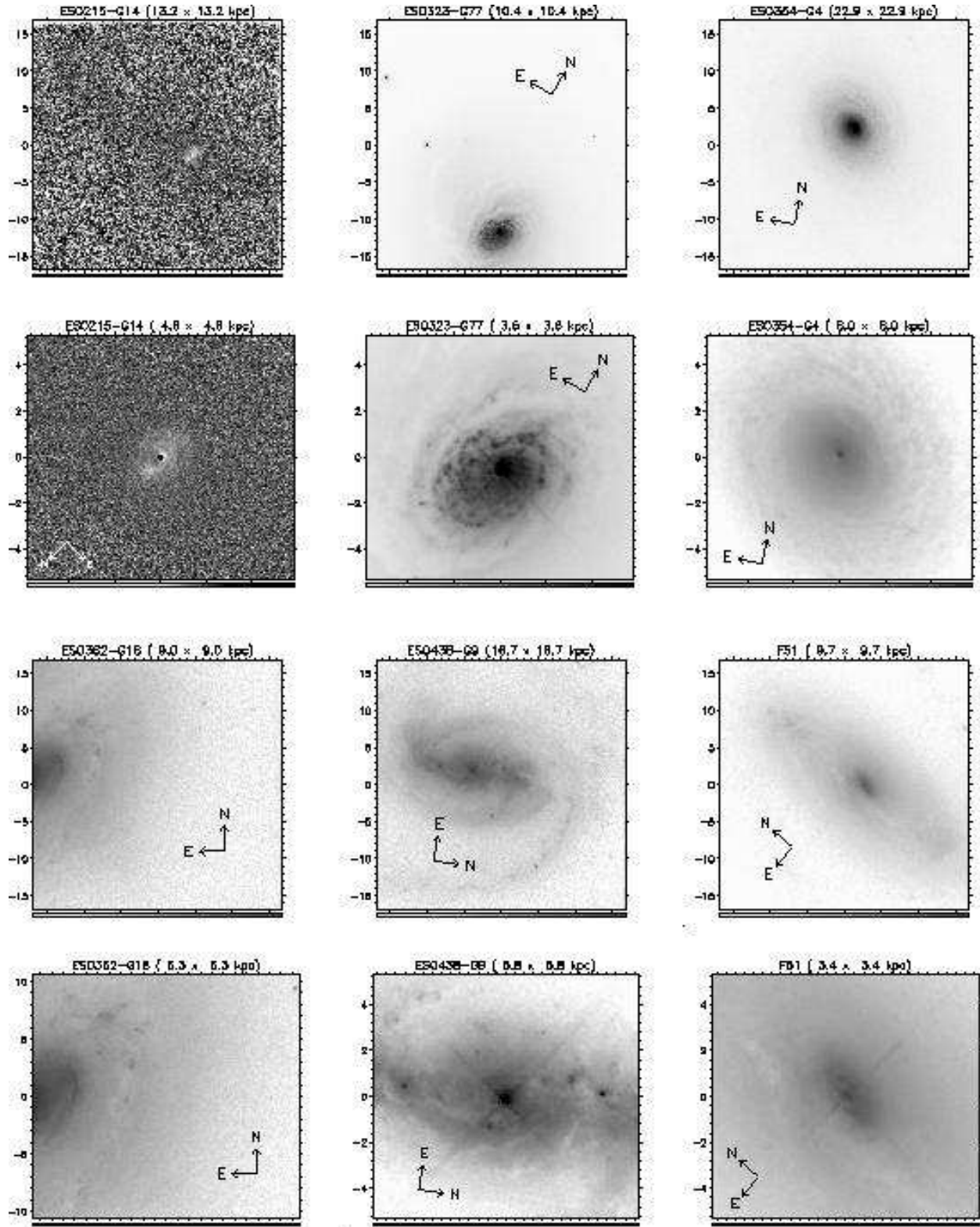


Fig. 2.— Structure maps of Seyferts 1s in Table 1

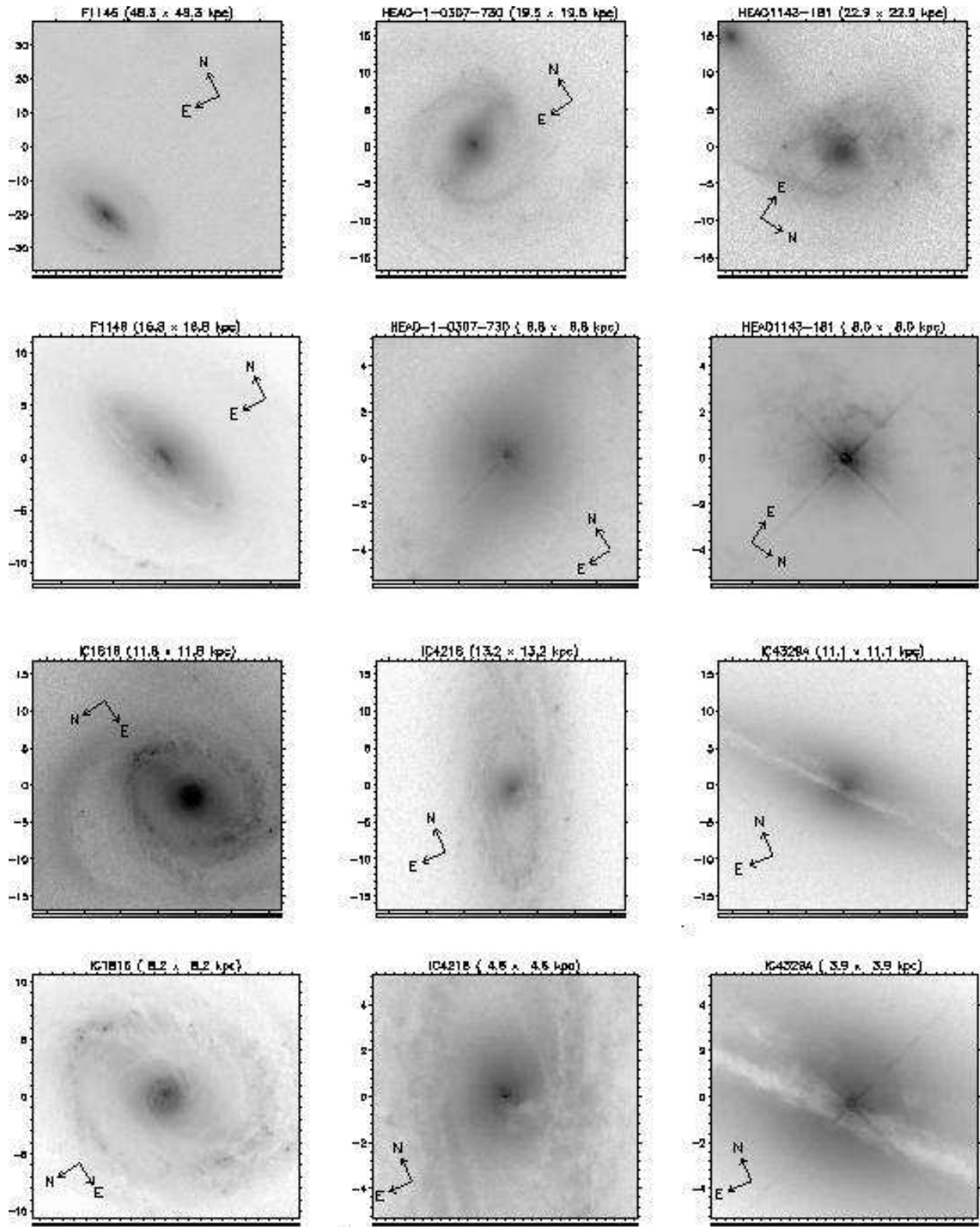


Fig. 2.— Continued

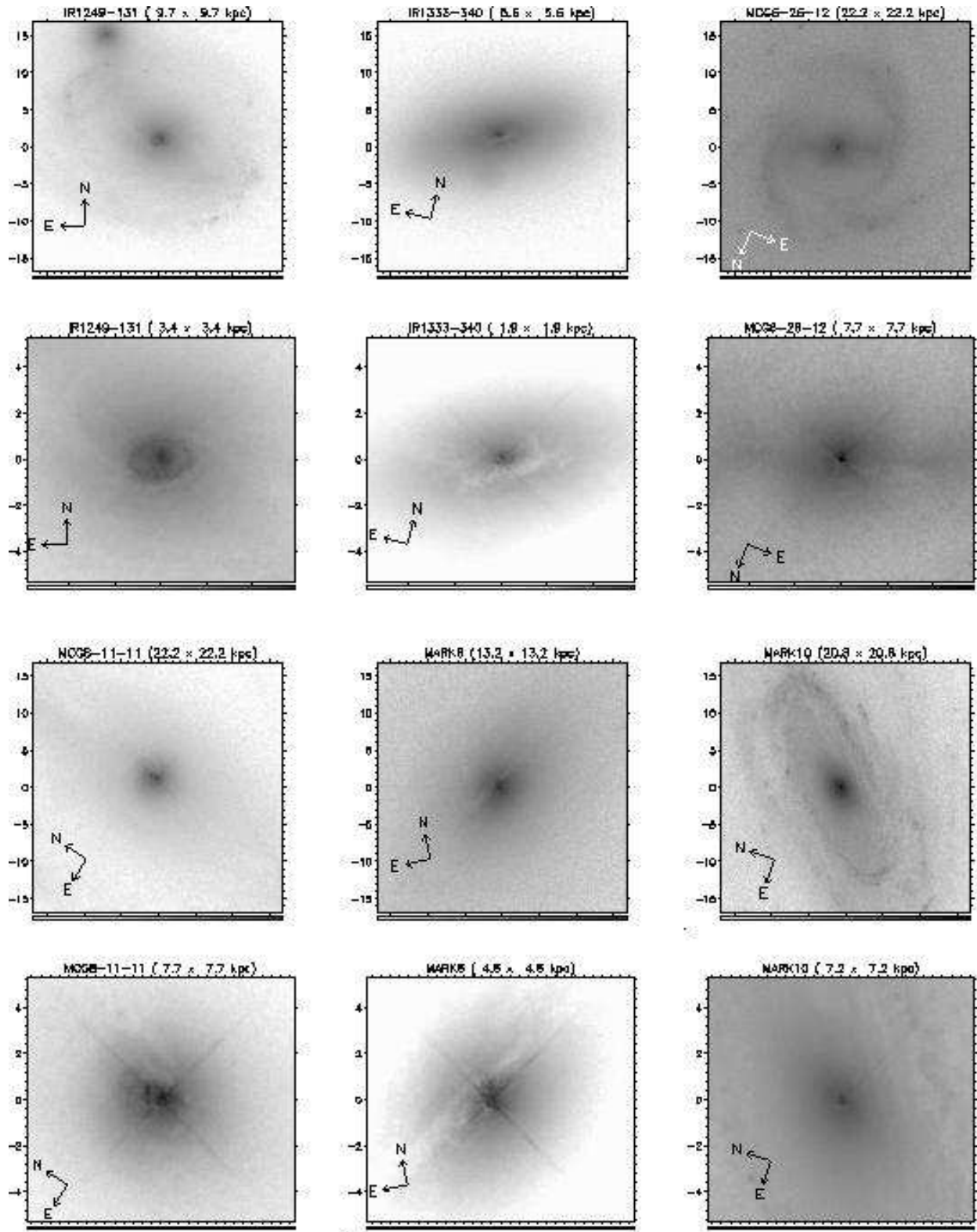


Fig. 2.— Continued

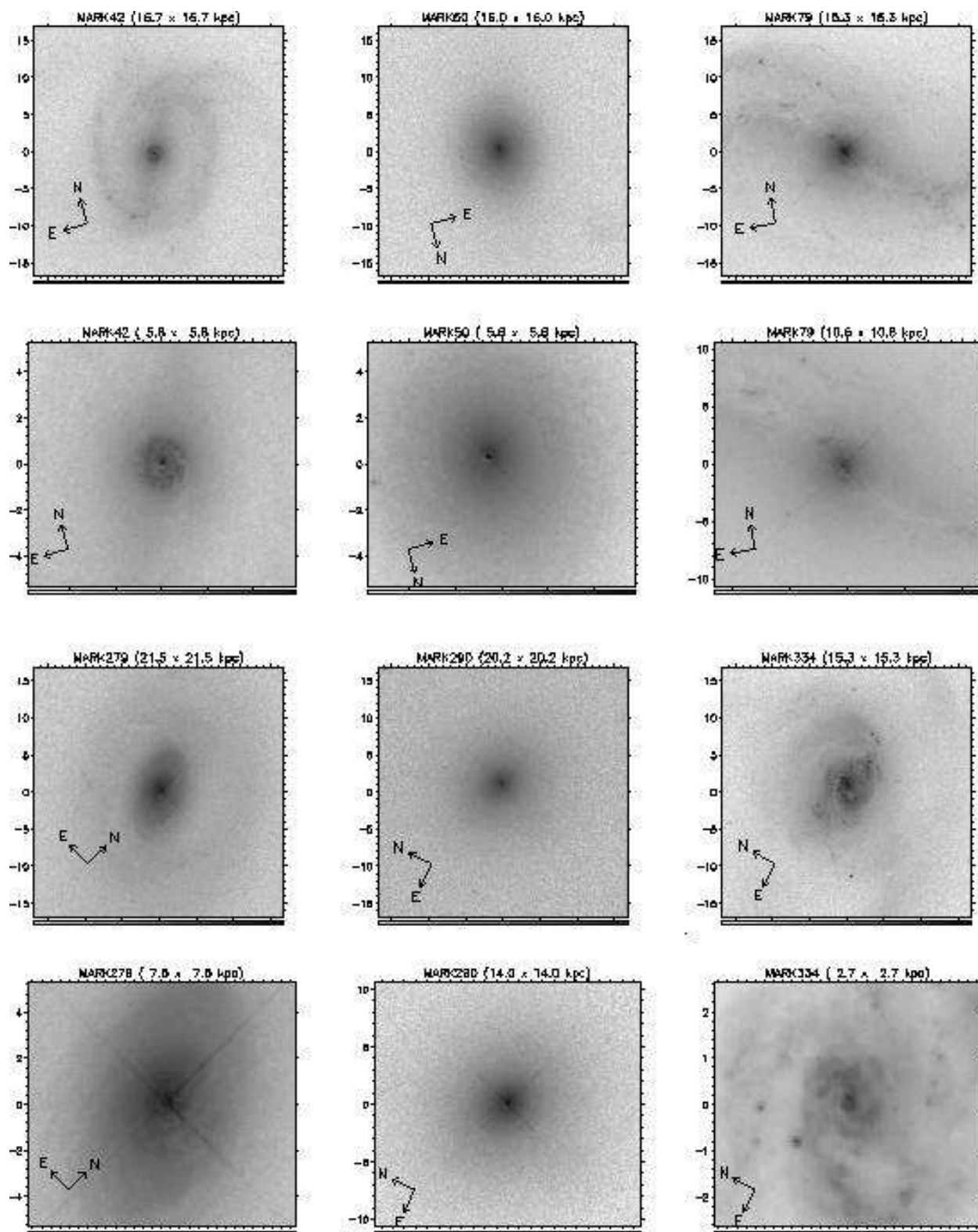


Fig. 2.— Continued

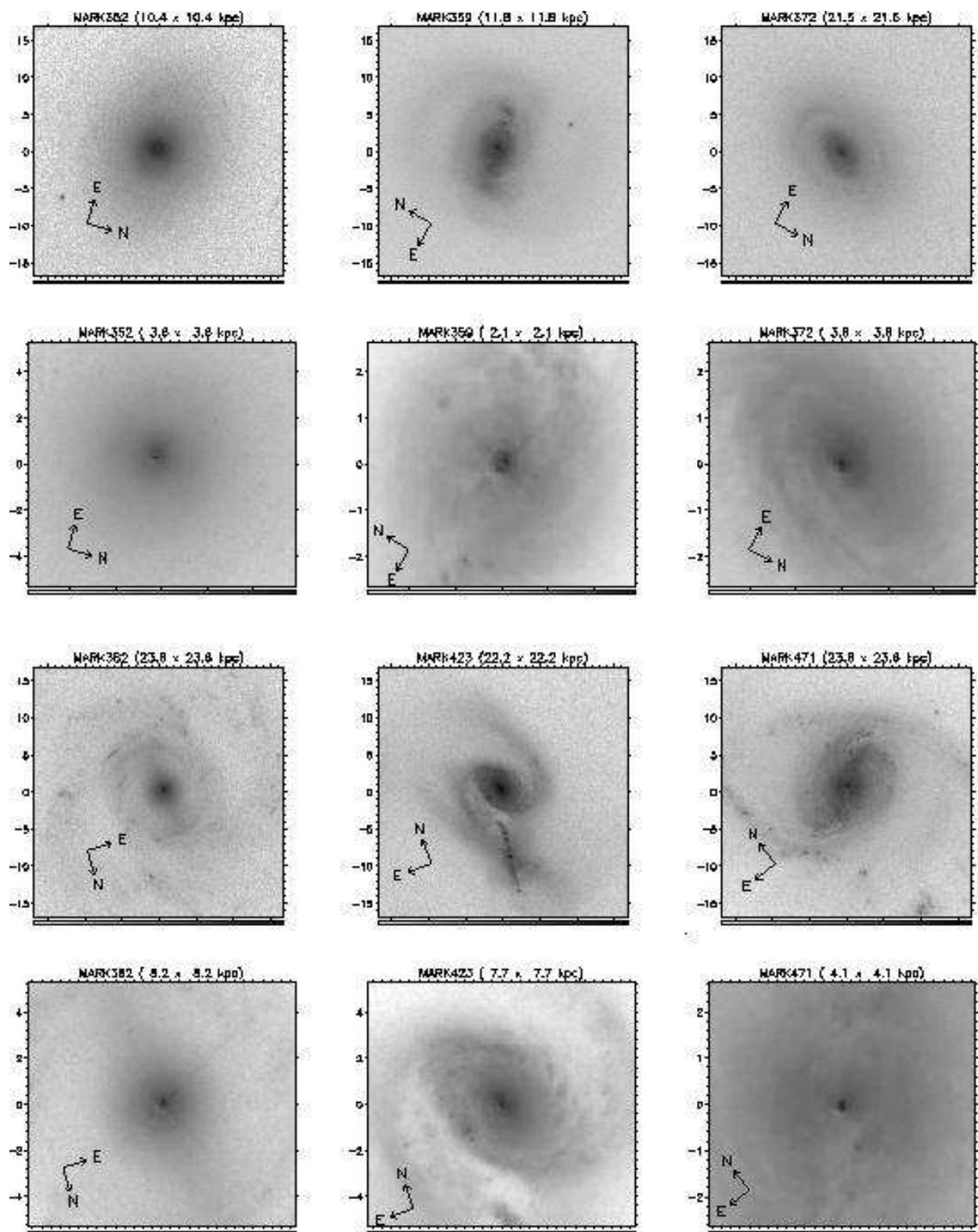


Fig. 2.— Continued

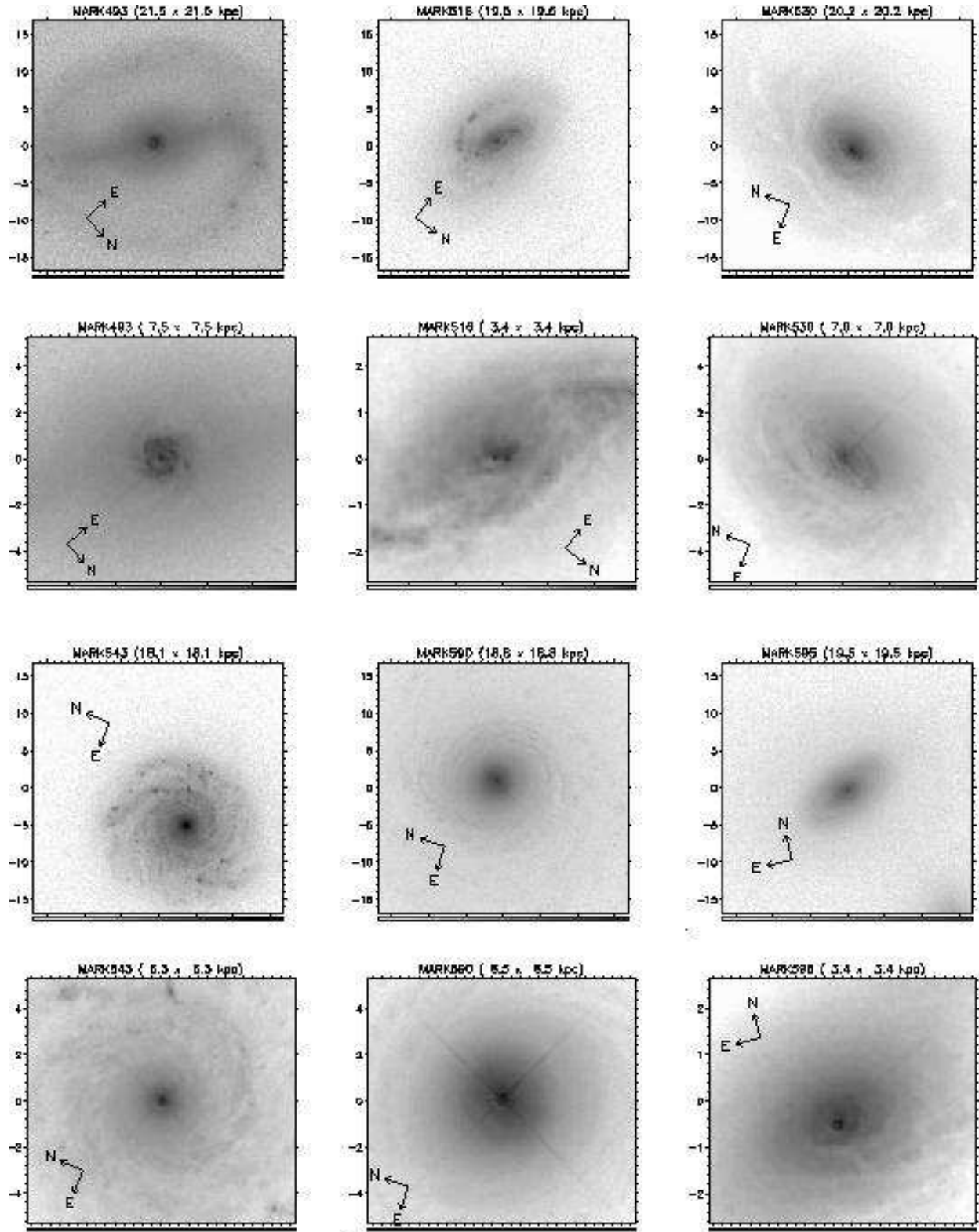


Fig. 2.— Continued

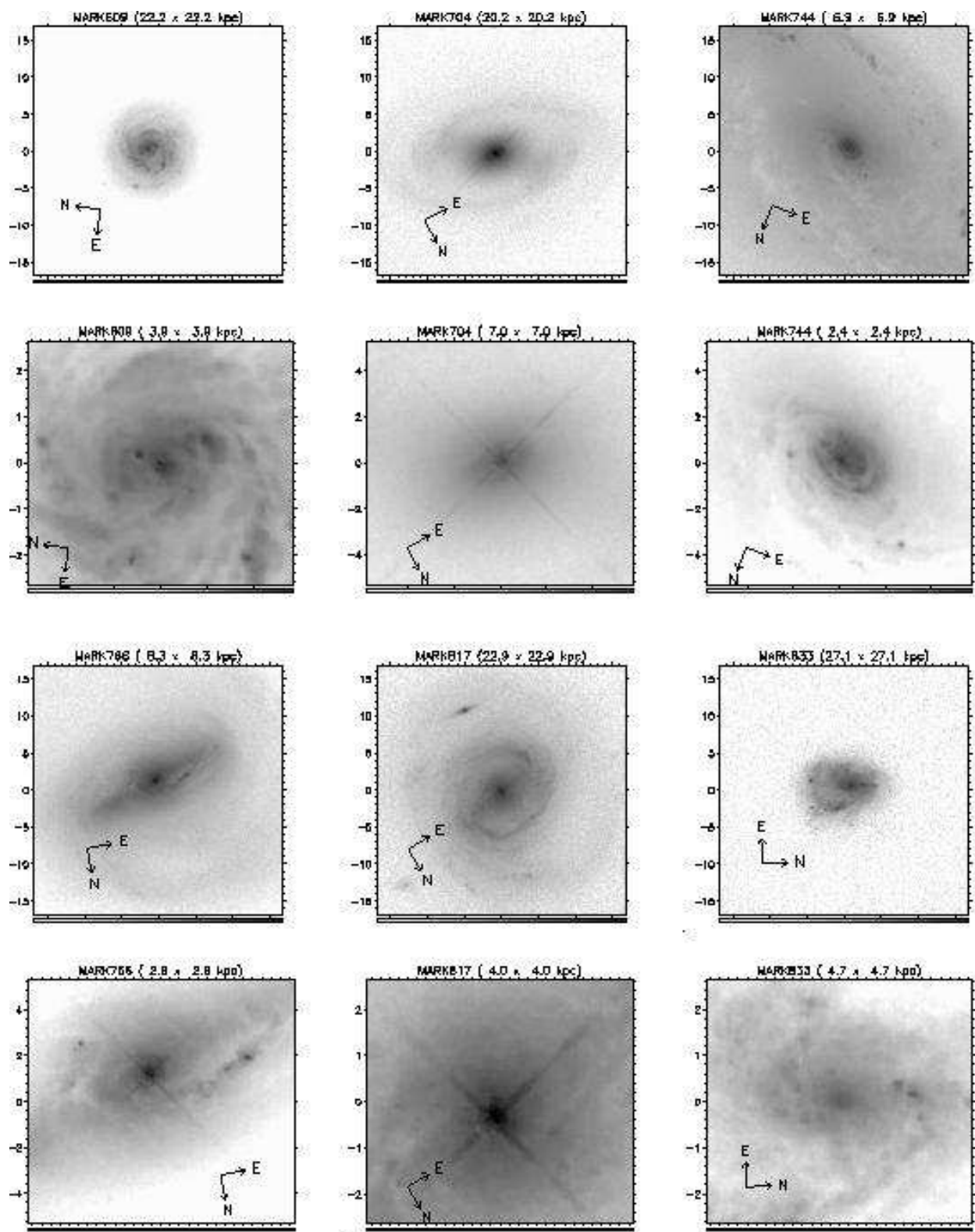


Fig. 2.— Continued

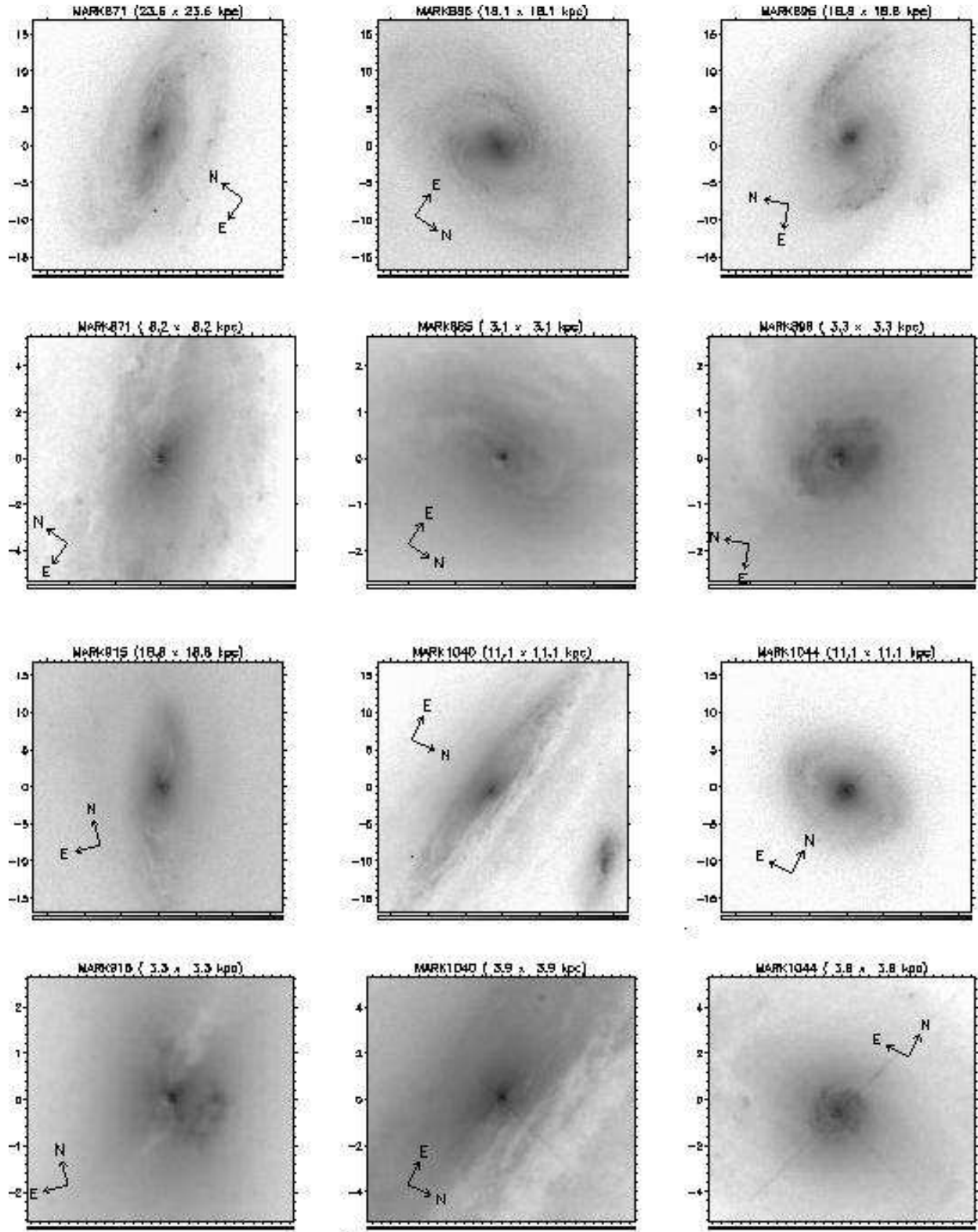


Fig. 2.— Continued

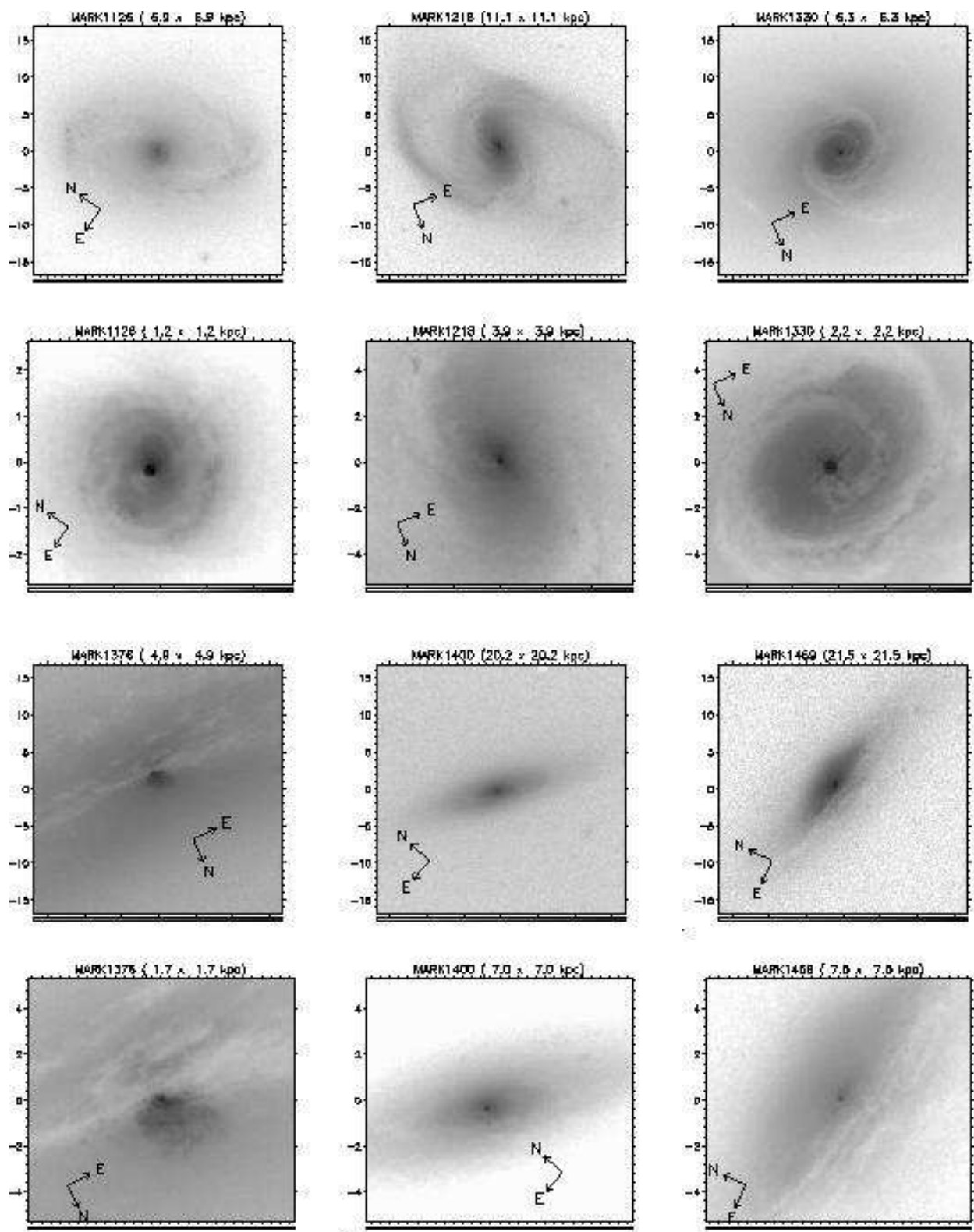


Fig. 2.— Continued

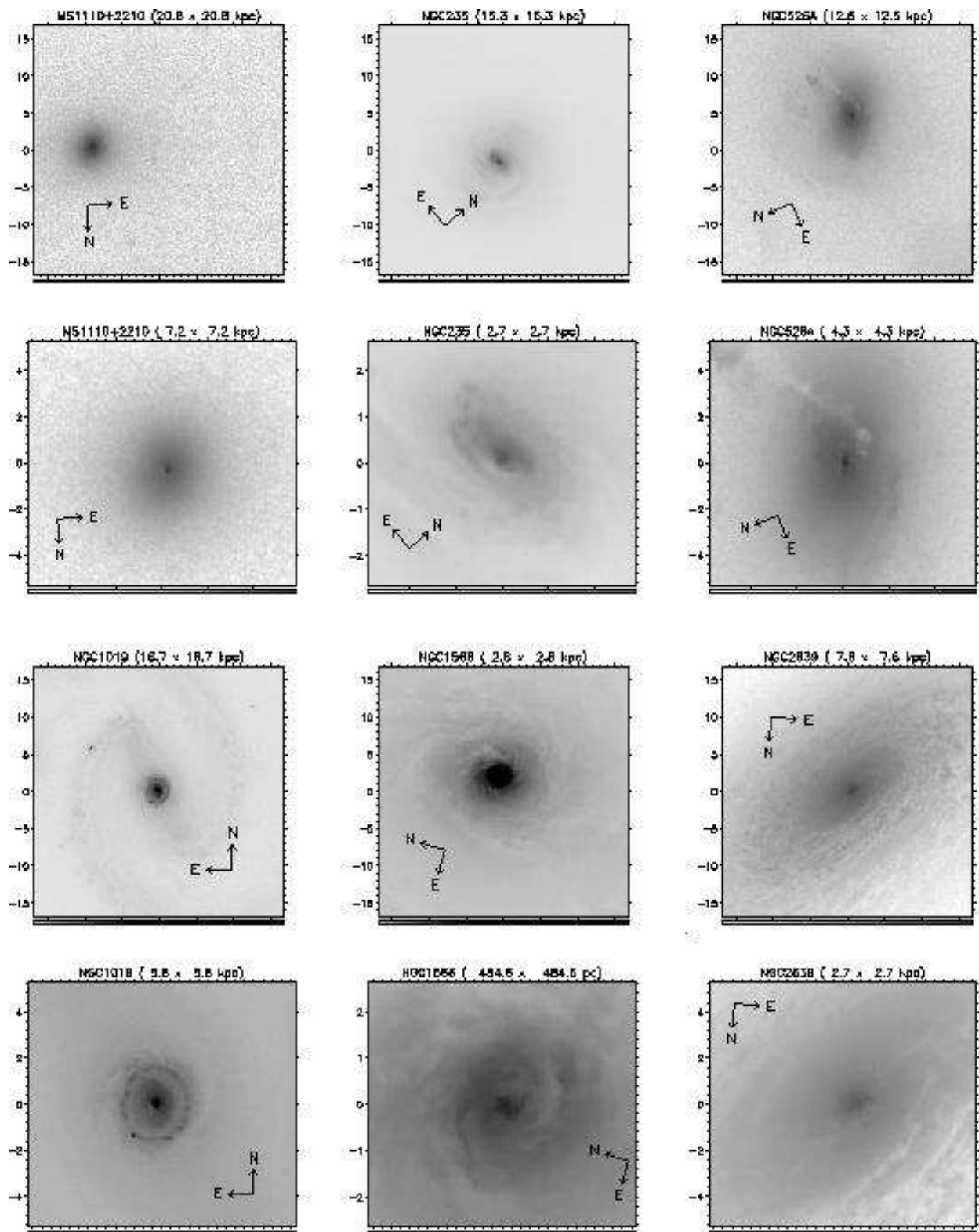


Fig. 2.— Continued

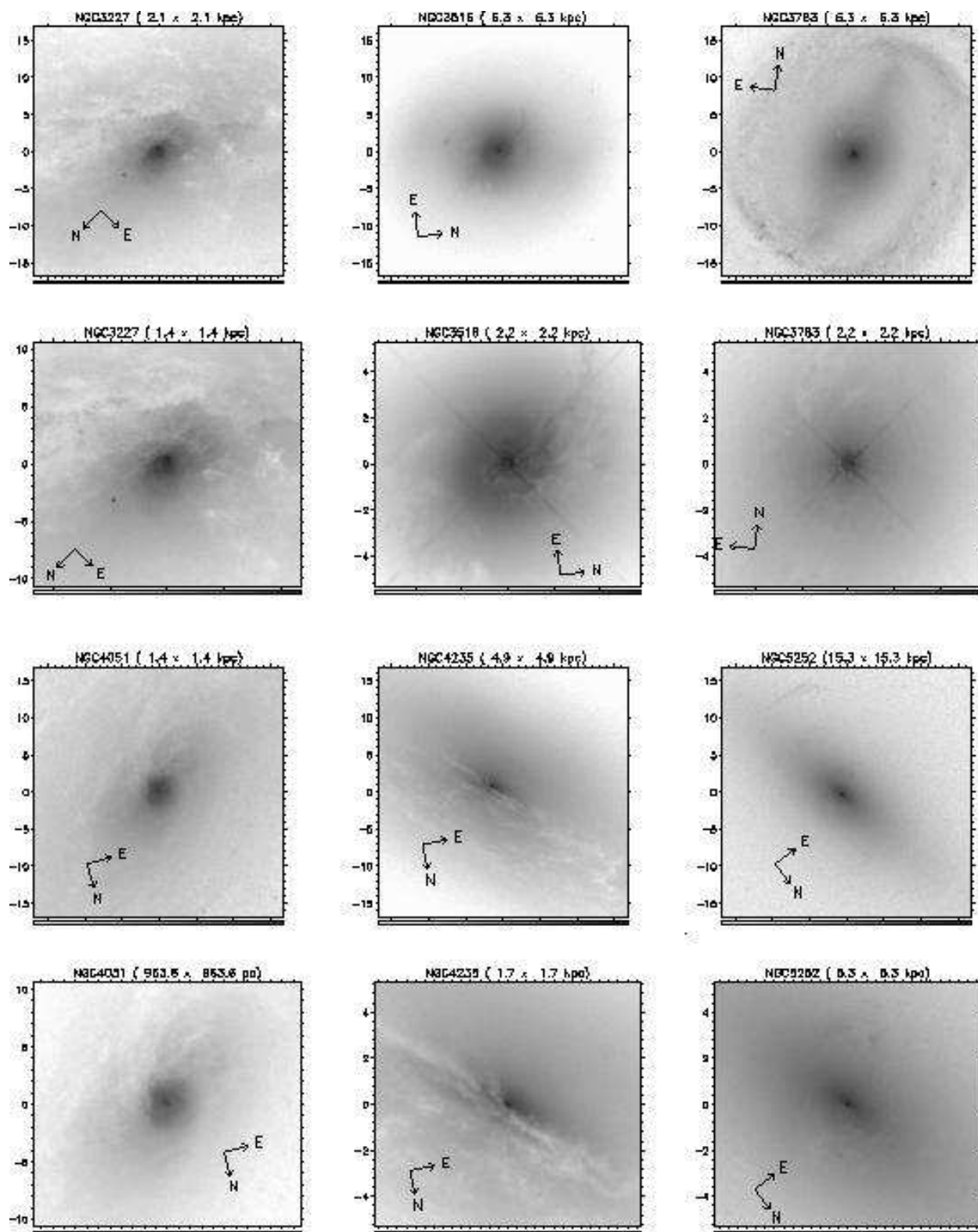


Fig. 2.— Continued

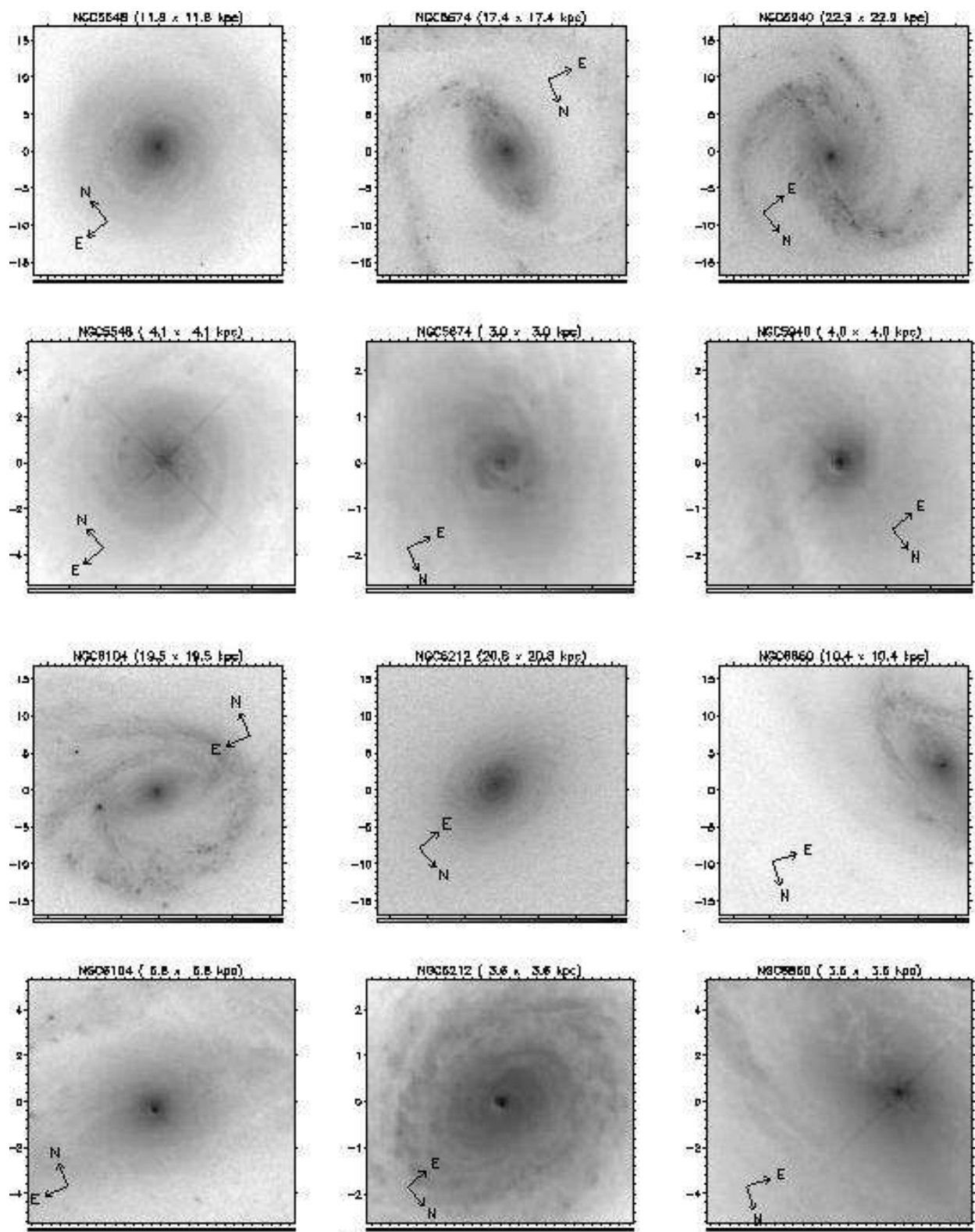


Fig. 2.— Continued

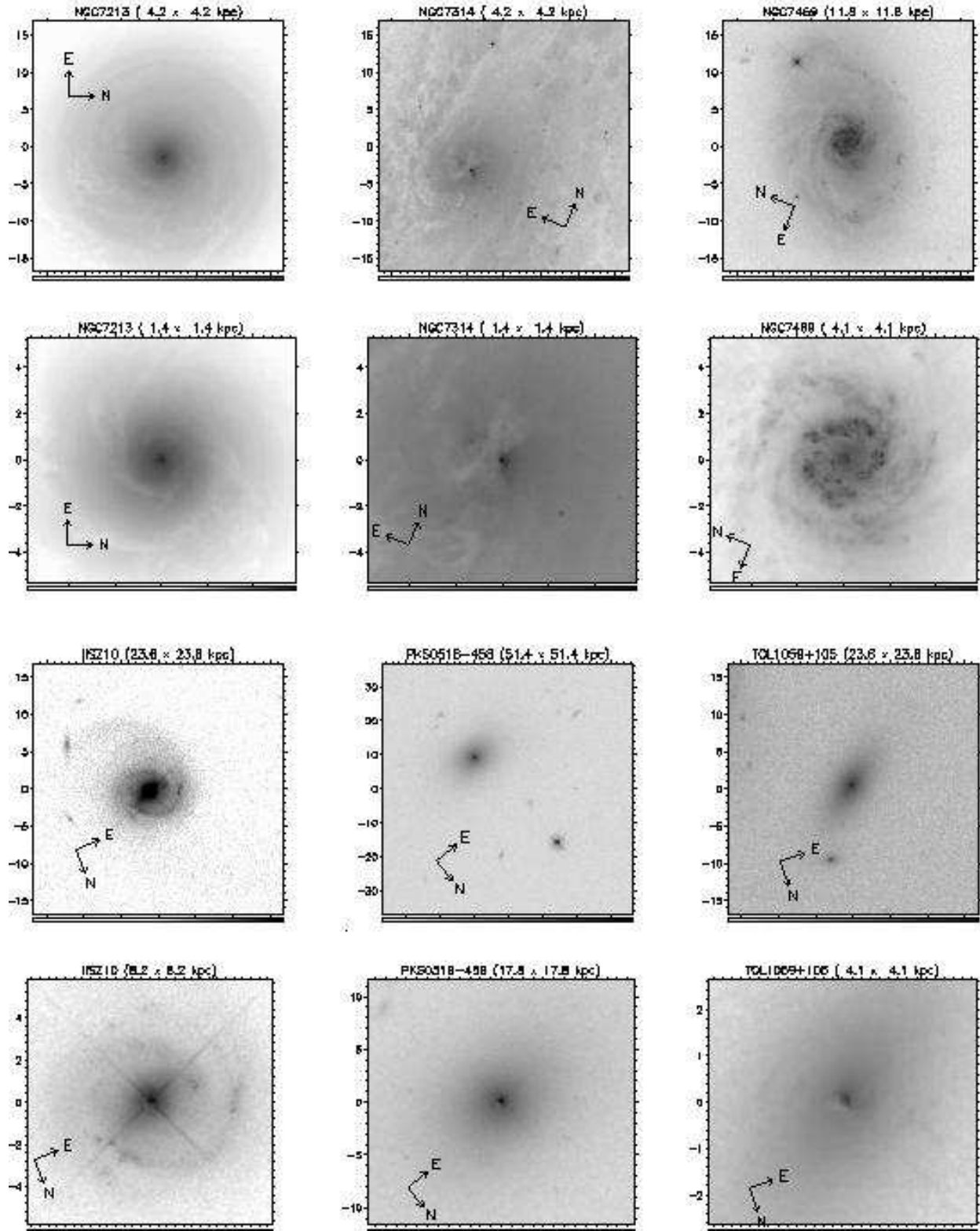


Fig. 2.— Continued

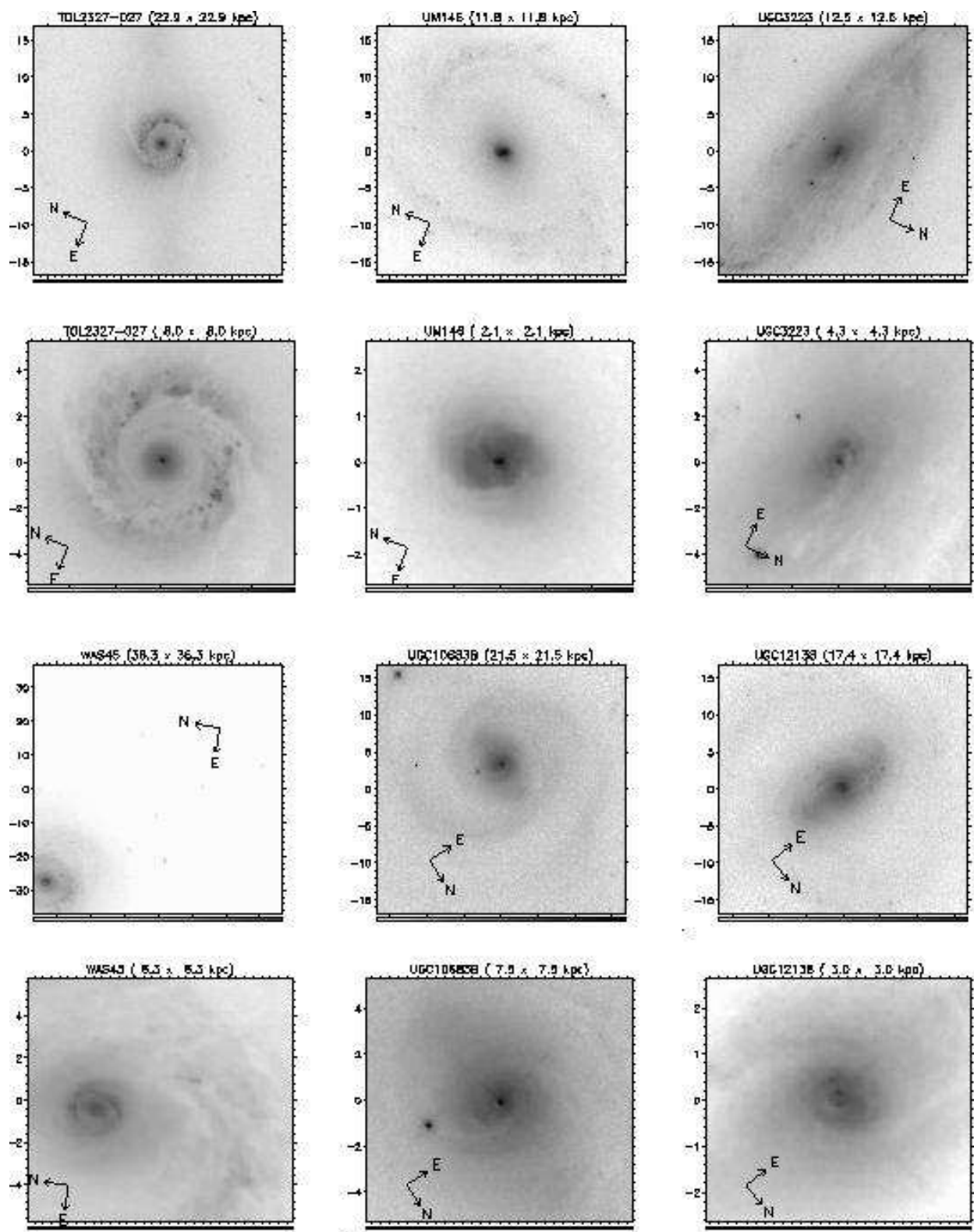


Fig. 2.— Continued

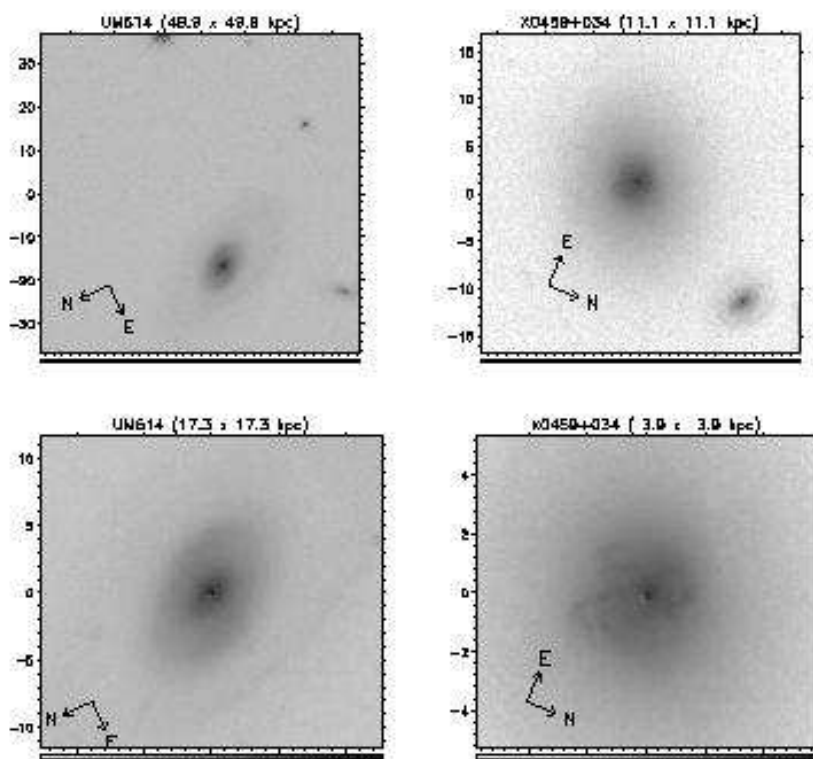


Fig. 2.— Continued

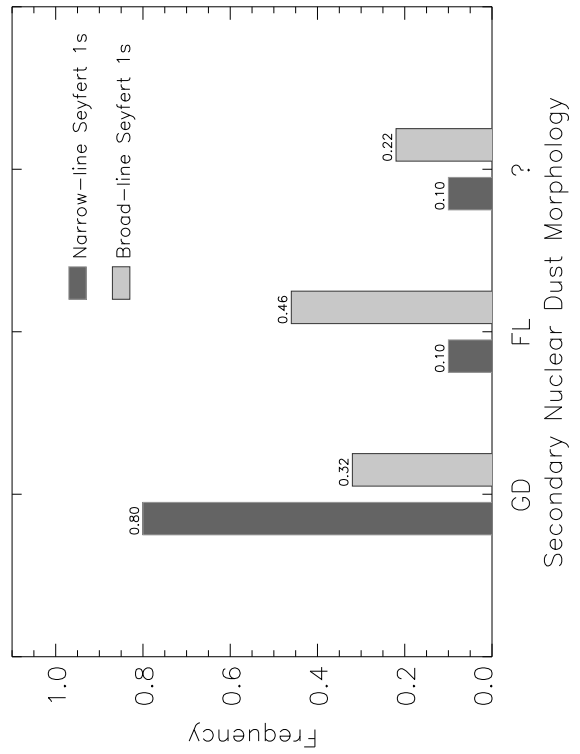
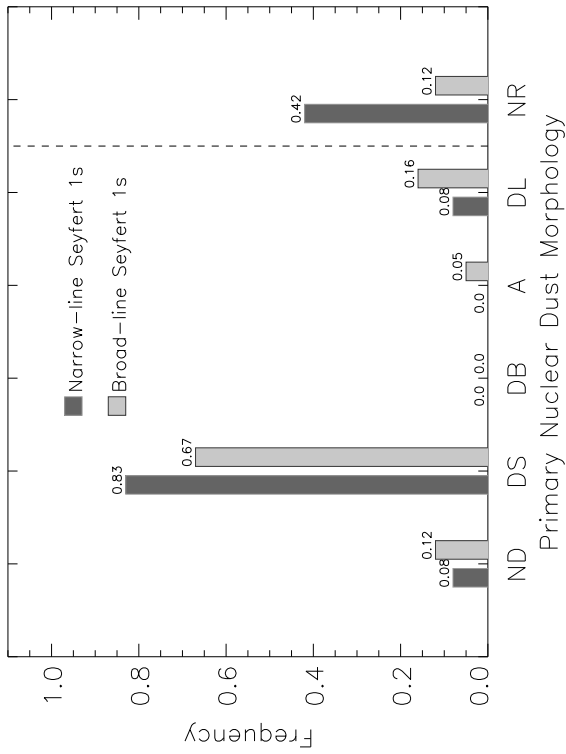
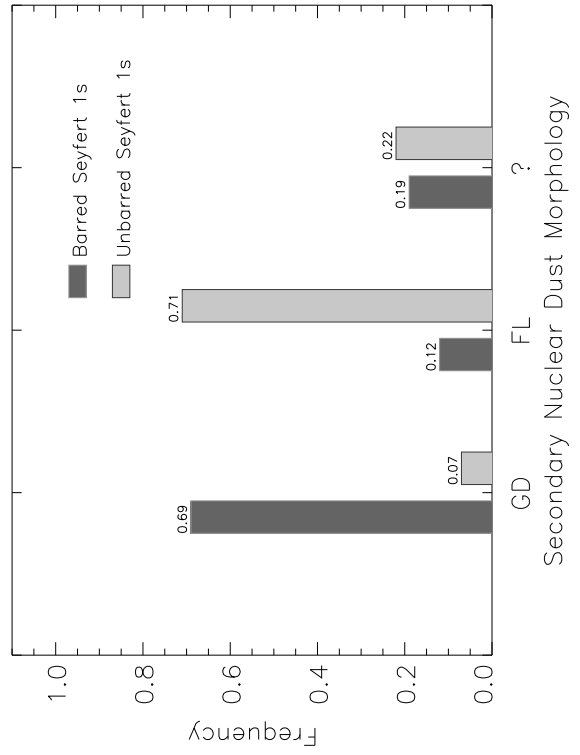
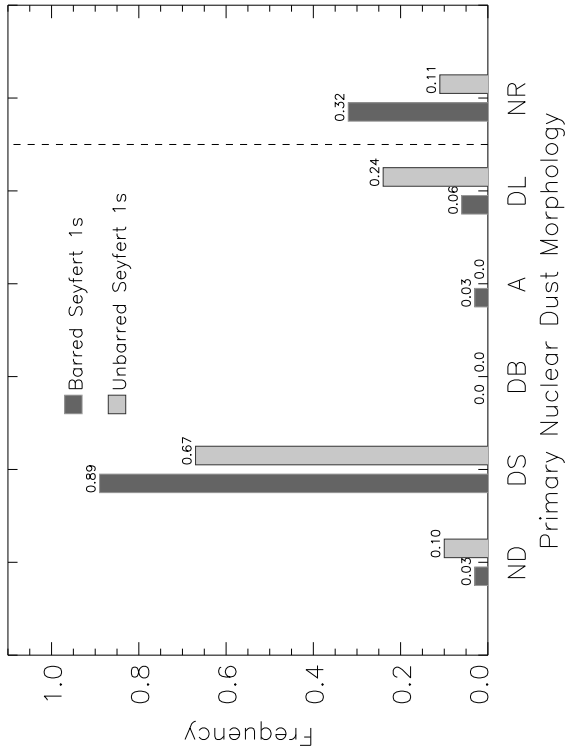


Fig. 3.— Frequency of Nuclear Dust Structures.